2016

Modeling hydrological controls on variations in peat water content, water table depth, and surface energy exchange of a boreal western Canadian fen peatland

Mezbahuddin, M.

American Geophysical Union

RESEARCH ARTICLE

Key Points:
- Substituting a Campbell model with a van Genuchten model into ecosys enabled better boreal fen peat moisture retention simulation
- Ecosys simulated wetter to drier season water table drawdown and peat drying in a boreal fen from vertical and lateral water exchanges
- Peat desiccation under a threshold water table depth simulated evapotranspiration reduction in a soil-plant-atmosphere hydraulic scheme

Correspondence to:
M. Mezbahuddin,
symon.mezbahuddin@gov.ab.ca

Modeling hydrological controls on variations in peat water content, water table depth, and surface energy exchange of a boreal western Canadian fen peatland

M. Mezbahuddin[1], R. F. Grant[2], and L. B. Flanagan[3]

[1]Environmental Stewardship Branch, Alberta Agriculture and Forestry, Edmonton, Alberta, Canada, [2]Department of Renewable Resources, University of Alberta, Edmonton, Alberta, Canada, [3]Department of Biological Sciences, University of Lethbridge, Alberta, Canada

Abstract Improved predictive capacity of hydrology and surface energy exchange is critical for conserving boreal peatland carbon sequestration under drier and warmer climates. We represented basic processes for water and O_2 transport and their effects on ecosystem water, energy, carbon, and nutrient cycling in a process-based model *ecosys* to simulate effects of seasonal and interannual variations in hydrology on peat water content, water table depth (WTD), and surface energy exchange of a Western Canadian fen peatland. Substituting a van Genuchten model (VGM) for a modified Campbell model (MCM) in *ecosys* enabled a significantly better simulation of peat moisture retention as indicated by higher modeled versus measured R^2 and Willmot's index (*d*) with VGM ($R^2 \sim 0.7$, $d \sim 0.8$) than with MCM ($R^2 \sim 0.25$, $d \sim 0.35$) for daily peat water contents from a wetter year 2004 to a drier year 2009. With the improved peat moisture simulation, *ecosys* modeled hourly WTD and energy fluxes reasonably well (modeled versus measured R^2: WTD ~0.6, net radiation ~0.99, sensible heat >0.8, and latent heat >0.85). Gradually declining ratios of precipitation to evapotranspiration and of lateral recharge to discharge enabled simulation of a gradual drawdown of growing season WTD and a consequent peat drying from 2004 to 2009. When WTD fell below a threshold of ~0.35 m below the hollow surface, intense drying of mosses in *ecosys* caused a simulated reduction in evapotranspiration and an increase in Bowen ratio during late growing season that were consistent with measurements. Hence, using appropriate water desorption curve coupled with vertical-lateral hydraulic schemes is vital to accurately simulate peatland hydrology and energy balance.

1. Introduction

Northern boreal and subarctic peatlands comprise 75–80% of total global peatland area [*Frolking et al.*, 2011] and have been accumulating soil carbon at a rate of 19–24 g m^{-2} yr^{-1} [*Clymo et al.*, 1998; *Vitt et al.*, 2000; *Gorham et al.*, 2003; *Turunen et al.*, 2004; *Roulet et al.*, 2007] over more than 6000 years [*Zoltai and Vitt*, 1990]. These peatlands have formed mainly due to slow decomposition in saturated soils under shallow or aboveground water table (WT). However, northern boreal peatlands are projected to shift from carbon sinks to sources as a result of water table depth (WTD) drawdown due to increased frequency and intensity of droughts over the upcoming millennium [*Frolking et al.*, 2011]. Deeper WT along with warmer weather can cause rapid aerobic decomposition in northern peatlands and hence can further contribute to atmospheric CO_2 [*Cai et al.*, 2010]. Moreover, WTD drawdown can hinder evapotranspiration (ET) due to drying of peat surfaces, and bryophytes (e.g., moss), and/or vascular plant water stress [*Dimitrov et al.*, 2011]. Intensive drying of mosses and/or vascular plant water stress can in turn cause reductions in gross primary productivity (GPP), thereby impeding peat accumulation [*Lafleur et al.*, 2005; *Dimitrov et al.*, 2011; *Peichl et al.*, 2014].

Seasonal and interannual variations in northern peatland WTD arise from variable balance among precipitation (*P*), ET, and lateral water fluxes in the forms of surface run-on/runoffs and subsurface recharge/discharge. However, WTD variations are not only affected by ET but also can affect peatland ET. This WTD-ET interaction is largely mediated by the moisture retention characteristics of a particular peat and its interaction with the peat-forming vegetation. Peats with low moisture-holding capacity can be rapidly drained with WTD drawdown. When WTD falls below a certain threshold level, capillary rise from WT becomes inadequate to supply moisture to mosses, which causes a reduction in moss evaporation (*E*). This WTD threshold depends upon moisture supplying capacity of a particular peat through capillary rise. Vascular plant roots, however, can penetrate into deeper peat layers and thus are expected to sustain water uptake and hence transpiration (*T*) during deeper

WT periods. If the reduction in moss E due to desiccation under deeper WT cannot be offset by sustained vascular T, the peatland ET declines [*Dimitrov et al.*, 2011]. However, when WT deepens past vascular root zones it can cause a reduction in vascular water uptake and hence canopy stomatal conductance (g_c), T, and GPP [*Lafleur et al.*, 2005; *Peichl et al.*, 2014]. Unlike peats with low moisture-holding capacity, those with high moisture-holding capacity can supply adequate moisture to the peat-forming vegetation through capillary rise. Consequently, water stress and hence reductions in ET and GPP due to similar drawdown of WTD are not common in peatlands, which are formed by peats with high moisture-holding capacity [*Parmentier et al.*, 2009; *Wu et al.*, 2010]. Therefore, the effects of WTD on ET vary across peatlands, depending upon the interaction among WTD, peat-specific soil moisture retention, and rooting depth of peat-forming vegetation.

WTD variations also determine the transition between aerobic and anaerobic zones and govern the O_2 status and energy yields for microbial and root respirations through its effects on peat moisture content and hence aeration. Peats that have low moisture-holding capacity can be drained rapidly with WTD drawdown that improves soil O_2 status and hence stimulates peat respiration [*Sulman et al.*, 2009, 2010; *Cai et al.*, 2010]. However, some peats can retain very high moisture content with deeper WTD, thus resulting in poorer peat drainage and O_2 status and hence less increase or no response of peat respiration to deeper WTD [*Parmentier et al.*, 2009; *Sonnentag et al.*, 2010].

Therefore, to better predict how northern boreal peatlands would behave under future drier and warmer climates it is imperative to have improved predictive capacity for the seasonal and interannual variations in the interactions between peatland hydrological and biogeochemical processes. To acquire this capacity, significant efforts have been made so far to test process-based models such as Dynamic Land Ecosystem Model [*Tian et al.*, 2010], Wetland-DeNitrification and DeComposition (DNDC) [*Zhang et al.*, 2002], ORganizing Carbon and Hydrology in Dynamic EcosystEms [*Krinner et al.*, 2005], McGill Wetland Model (MWM) [*St-Hilaire et al.*, 2010], Lund-Potsdam-Jena [*Sitch et al.*, 2003; *Gerten et al.*, 2004], Peatland Carbon Simulator [*Frolking et al.*, 2002], Biome-BioGeochemical Cycles [*Bond-Lamberty et al.*, 2007], Simple Biosphere/Carnegie-Ames-Stanford Approach [*Schaefer et al.*, 2008], Boreal Ecosystem Productivity Simulator [*Sonnentag et al.*, 2008], Forest-DNDC [*Kurbatova et al.*, 2009], Terrestrial ECOsystem [*Weng and Luo*, 2008], PEATLAND [*van Huissteden et al.*, 2006], and Simple Biosphere [*Baker et al.*, 2008] in simulating hydrological feedback to peatland C processes across northern boreal peatlands. Although Wetland version of Canadian Land Surface Scheme (CLASS3W)-MWM [*Wu et al.*, 2012; *Wu and Roulet*, 2014] simulates prognostic WT, the other models either (1) do not have prognostic WT that prevents simulation of a continuous anaerobic zone below WT [*Baker et al.*, 2008; *Schaefer et al.*, 2008; *Tian et al.*, 2010] or (2) do not simulate peat saturation since any water in excess of field capacity is drained [*Gerten et al.*, 2004; *Krinner et al.*, 2005; *Weng and Luo*, 2008]. This hinders those models' ability to simulate R_e suppression under saturated conditions and hence peat formation [*Sulman et al.*, 2012].

Prognostic WT in process-based peatland models can be simulated from hydraulically driven vertical and lateral water fluxes. However, northern peatlands differ between two major classes, i.e., fens and bogs, in terms of lateral water exchange [*Tarnocai*, 2006]. Fens are known to receive water laterally from surrounding mineral soil WT, whereas bogs are entirely precipitation fed. So process-based modeling of fen WTD variation poses an additional challenge in accounting for lateral water inflow from adjacent upland ecosystems. *Bond-Lamberty et al.* [2007] accounted for this lateral inflow as a function of P while simulating site-specific lateral water gain in a poorly drained forest of Manitoba, Canada. However, a more universal solution of a hydraulically driven lateral water transfer scheme based on Darcy's law in a process-based ecosystem model *ecosys* simulated lateral water exchange of a northern boreal fen peatland [*Grant et al.*, 2012] and a boreal peat-mineral soil transitional ecotone [*Dimitrov et al.*, 2014] reasonably well.

WTD variation affects seasonal and interannual variations in peat moisture content depending upon peat moisture retention characteristics. Peat moisture retention in current peatland models are predominantly simulated from numerical solutions of soil moisture contents as functions of heights above the WT (i.e., soil matric water potential, ψ_m) using either a linear [e.g., *Zhang et al.*, 2002; *Barr et al.*, 2012] or a Campbell-type [*Campbell*, 1974] power function [*Frolking et al.*, 2002; *St-Hilaire et al.*, 2010]. Most of the current peatland models that do not simulate a prognostic WT use site-measured WTD as inputs in these numerical solutions [e.g., *Frolking et al.*, 2002; *Zhang et al.*, 2002; *Kurbatova et al.*, 2009; *St-Hilaire et al.*, 2010; *Barr et al.*, 2012]. A more complex process-based model *ecosys* simulates a prognostic WT that affects soil moisture retention
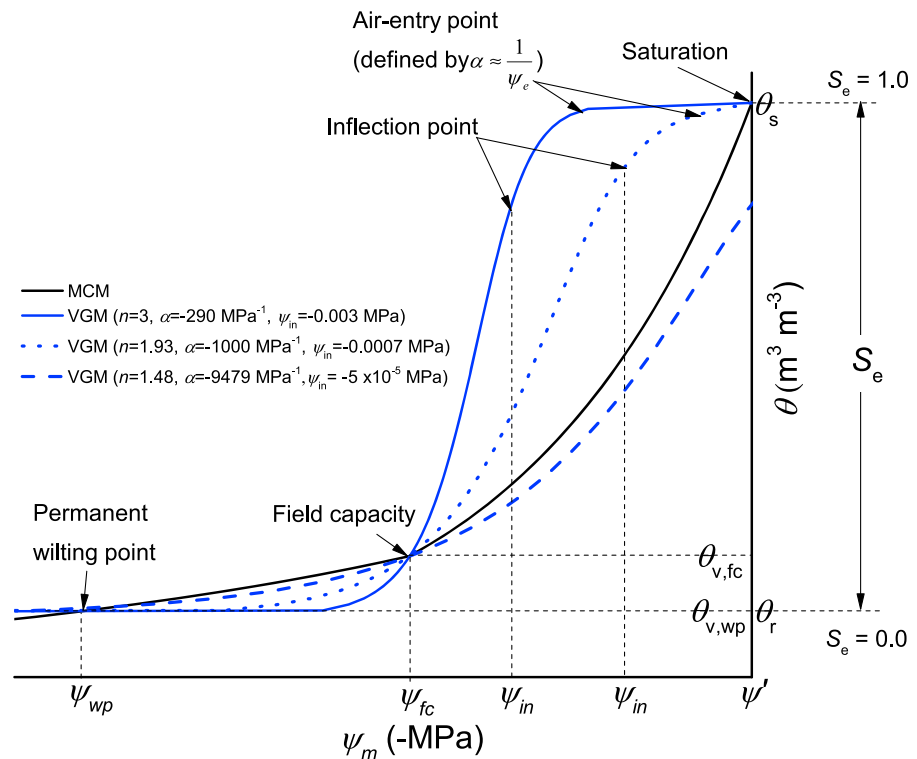
Figure 1. Hypothetical curves for van Genuchten (VGM) and modified Campbell (MCM) soil moisture desorption functions. S_e = relative degree of saturation, θ = ambient volumetric soil water content, θ_s = volumetric soil water content at saturation, $\theta_{v,fc}$ = volumetric soil water content at field capacity, $\theta_{v,wp}$ = volumetric soil water content at wilting point, θ_r = residual soil water content, ψ_m = soil matric water potential, ψ' = ψ_m at saturation, ψ_e = air-entry potential, ψ_{in} = ψ_m at the inflection point, ψ_{fc} = ψ_m at field capacity, ψ_{wp} = ψ_m at wilting point, n and α = VGM shape parameters.

through a log-transformed Campbell model (defined as a modified Campbell model or MCM hereafter), which enabled the model to simulate peat moisture retention reasonably well in a northern boreal bog [*Dimitrov et al.*, 2010] and a tropical bog [*Mezbahuddin et al.*, 2015]. The Campbell equation or its modification(s) (e.g., MCM in *ecosys*) usually results in a hyperbolic relationship (*J* shape) between soil moisture content (θ) and ψ_m while simulating soil moisture desorption with declining ψ_m (Figure 1). However, many peats have moisture retention characteristics that follow sigmoidal (*S*-shape) logistic curves [e.g., *Päivänen*, 1973; *Weiss et al.*, 1998; *Gnatowski et al.*, 2010; *Dettmann et al.*, 2014] with inflection points (ψ_{in}; Figure 1). Application of soil moisture desorption equations like the Campbell model or its modification(s) in simulating these types of peat moisture retention could thus lead to a significant underestimation of near-saturation peat water contents (Figure 1). This in turn could cause a substantial overestimation of peat aeration and hence respiration in those peatlands.

A van Genuchten-type [*van Genuchten*, 1980] soil moisture retention function can address this challenge by simulating sigmoidal or *S*-shaped moisture desorption curves with regressing ψ_m (Figure 1). The van Genuchten model (VGM) is in fact the most commonly used soil moisture retention equation in current hydrological modeling of mineral soils [*Dettmann et al.*, 2014]. Beside sigmoidal curves, VGM can also simulate *J*-shaped moisture retention curves similar to the Campbell model [*Silins and Rothwell*, 1998; *Weiss et al.*, 1998] and hence is suggested to be the most suitable one for moisture retention modeling across peatlands [*Dettmann et al.*, 2014]. *Letts et al.* [2000] developed parameters that were designed for the soil moisture characteristics curves for fibric, hemic, and sapric peat using VGM formulation to be employed in the 1-D Canadian Land Surface Scheme (CLASS). *Schwärzel et al.* [2006] used VGM to simulate a German drained fen peatland hydrology in a 1-D HYDRUS soil-plant-atmosphere moisture scheme. Therefore, investigating the applicability of VGM in simulating peat θ variations while coupled with a detailed 3-D soil-plant-atmosphere moisture scheme in *ecosys* would further improve our predictive capacity of seasonal and inter-annual variations in peat moisture retention.

Variation in θ as affected by variation in WTD can affect peatland ET and hence GPP. The effects of peat moisture retention on peatland ET and GPP in most of the current peatland models are computed by using scalar functions to account for moisture limitations to ET and GPP under either very dry or wet soil conditions [e.g., *Frolking et al.*, 2002; *Zhang et al.*, 2002; *Bond-Lamberty et al.*, 2007; *St-Hilaire et al.*, 2010; *Sulman et al.*, 2012]. This approach may not be robust because soil-vegetation-climate moisture feedback vary across peatlands depending upon the interaction between peat moisture retention and peat-forming vegetation as discussed above [*Lafleur et al.*, 2005; *Parmentier et al.*, 2009; *Wu et al.*, 2010; *Sonnentag et al.*, 2010; *Dimitrov et al.*, 2011; *Peichl et al.*, 2014], so that these scalar functions need to be parameterized for every site. So to improve our predictive capacity of variable WTD feedback to ET across peatlands we need a more universal solution of peatland ET while equilibrating vegetation-atmosphere moisture exchange with vegetation water uptake in a soil-plant-atmosphere hydraulic scheme. Instead of using site specifically parameterized scalar functions, this hydraulic scheme can equilibrate atmospheric ET demand from surface and canopy energy balances with moisture supply by vegetation as mediated by (1) rooting profiles resulting from root-WTD interactions and (2) a series of water potentials (e.g., soil, root, and canopy water potentials) and hydraulic resistances (soil, root, canopy surface, and/or stomatal resistances) [*Dimitrov et al.*, 2011; *Mezbahuddin et al.*, 2015].

1.1. Objectives and Rationale

Given the importance of interactions among WTD, peat moisture retention and peat-forming vegetation in modeling WTD effects on ET and GPP across peatlands, the present study aims at using a process-based ecosystem model *ecosys* (1) to examine the applicability of the van Genuchten model in improving simulation of peat moisture desorption, (2) to simulate seasonal and interannual variations of WTD by coupling vertical and lateral water fluxes determined by the improved moisture retention and water exchange through vertical and lateral model boundaries, and (3) to simulate and thereby better understand the effects of seasonal and interannual variations in soil moisture and WTD on surface energy exchange while modeling process-based feedback between hydrology and ecology of a Western Canadian boreal fen peatland [*Syed et al.*, 2006; *Flanagan and Syed*, 2011] in Alberta, Canada.

Improvement of peat moisture simulation in this study would be accomplished by replacing the existing moisture retention function (MCM) in *ecosys* with the VGM and testing the VGM versus MCM daily outputs for θ against daily site measurements. With the improved moisture retention function, *ecosys* outputs of hourly WTD and energy fluxes (e.g., latent and sensible heat fluxes) would then be tested against site measurements to examine how well *ecosys* would simulate seasonal and interannual variations in WTD and surface energy exchange of the Western Canadian peatland (WPL) site. After the testing of modeled outputs against measurements, comparative studies of modeled and measured WTDs and surface energy exchange would be performed between shallow and deep WTD periods to examine and explain WTD effects on surface energy exchange of WPL. This rigorous testing of model outputs against measurements as well as examination of contrasting responses of surface energy exchange between different WTD periods is likely to improve our predictive capacity and insights of how the northern boreal fen peatland ecohydrology would be affected by future drier climates.

1.2. Hypotheses
1.2.1. Hypothesis 1: van Genuchten Model (VGM) Versus Modified Campbell Model (MCM) in Simulating Peat Moisture Desorption

Numerical solution of ψ_m as a function of θ in a log-transformed Campbell model (MCM; Figure 1) enabled *ecosys* to successfully simulate near-surface peat θ in a boreal bog [*Dimitrov et al.*, 2010] and a tropical bog [*Mezbahuddin et al.*, 2015] peatland. Those peats had low near-saturation moisture-holding capacity and hence exhibited rapid pore drainage immediately below saturation, thereby matching the *J*-shaped moisture retention curve in MCM when simulating decreasing θ with declining ψ_m (Figure 1). However, unlike those bog peats, fen peat at the WPL site retained high θ close to saturation and drained rapidly when declining WTD caused ψ_m to decrease below a threshold (i.e., air entry potential, ψ_e), thereby producing a sigmoidal (*S*-shape) moisture retention curve [*Cai et al.*, 2010; *Long et al.*, 2010]. Since VGM simulates sigmoidal moisture desorption curves, we hypothesize that substituting MCM with VGM in *ecosys* would better simulate peat θ measured in WPL. This test of VGM versus MCM in *ecosys* for simulating peat θ would improve our predictive capacity of peat moisture retention across peatlands.

1.2.2. Hypothesis 2: Modeling Variation in WTD from Balance Between Vertical and Lateral Water Fluxes

Variation in peat θ is also affected by changes in site hydrology that affect variation in WTD that in turn affects ψ_m. A drying trend was evident at the WPL from gradual drawdown of growing season (May–August) WTD from the wettest growing season of 2004 to the driest growing season of 2009 [*Flanagan and Syed*, 2011]. We hypothesize that *ecosys* would be able to simulate this gradual drawdown of WTD from gradually decreasing vertical influx (*P*) to efflux (ET) and lateral influx (recharge) to efflux (discharge) ratios.

1.2.3. Hypothesis 3: Modeling Effects of WTD Variation on Ecosystem Energy Exchange

Gradual WTD drawdown from the wettest (2004) to the driest (2009) growing season (May–August) at the WPL also caused ecosystem drying. This was evaluated by a rapid decline in growing season eddy covariance (EC) actual/potential ET estimates when average growing season WT fell below a threshold level during drier growing seasons of 2008 and 2009 compared to other growing seasons (e.g., 2004–2007) [*Flanagan and Syed*, 2011]. We hypothesize that *ecosys* would be able to model this threshold WTD response to ET in the WPL by simulating feedback between WTD and ET as mediated by vertical water fluxes controlled by the interaction between plant water relations and soil moisture retention improved with the use of VGM.

2. Methods

2.1. Model Development

Ecosys is a process-based terrestrial ecosystem model that successfully simulated 3-D water, energy, carbon, and nutrient (N, P) cycles across a variety of peatlands [*Dimitrov et al.*, 2010, 2011; *Grant et al.*, 2012; *Mezbahuddin et al.*, 2014, 2015]. *Ecosys* algorithms that govern simulations of soil moisture retention, WTD, and surface energy exchange which are related to our hypotheses are described below. The equations that are listed in the Appendices A–H in the supporting information are cited in the text within round brackets with a letter representing a particular appendix followed by the equation number.
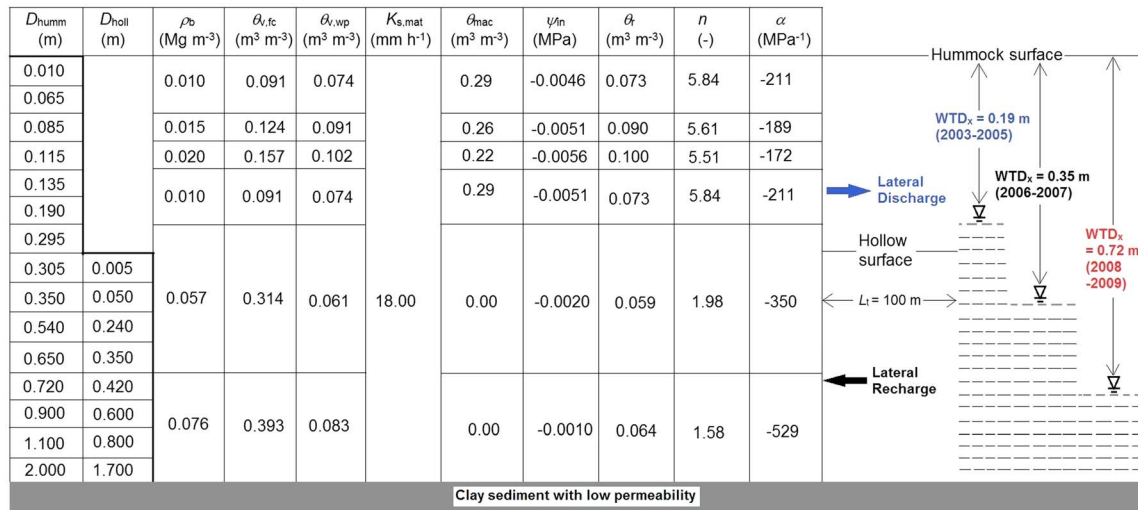
2.1.1. Water Table Depth (WTD)

The WTD in *ecosys* is calculated at the end of each time step as the depth to the top of the saturated zone below which air-filled porosity is zero (C1). This WTD is the depth at which lateral water flux is in equilibrium with the difference between vertical influxes (*P*) and effluxes (ET). The WTD in *ecosys* is thus not prescribed, but rather controls, and is controlled by lateral and vertical surface and subsurface water fluxes (A1–A7, B1–B5, and B18–B24).

2.1.2. Lateral Water Fluxes

Lateral surface runoff within the modeled grid cells and across lower surface boundaries is modeled using Manning's equation (A2) with surface water velocity (A3) calculated from surface geometry (A4) and slope (A5) and with surface water depth (A2) calculated from surface water balance (A1) using kinematic wave theory. Lateral subsurface flow in *ecosys* is governed by the lateral subsurface boundary condition. This lateral subsurface boundary condition in *ecosys* is defined by a specified external WTD (WTD$_x$) and a specified lateral distance (L$_t$) over which lateral subsurface water flow occurs (Figure 2). The WTD$_x$ represents average WTD of the surrounding watershed with which modeled boundary grid cells exchange water. The lateral water fluxes are governed by the hydraulic gradient between the WTD within the modeled grid cell and WTD$_x$ over L$_t$ in a Darcy's equation and by macropore and matrix hydraulic conductivity of the soil layer in which these fluxes occur (Figure 2). Thus, when WTD within modeled grid cells is shallower than WTD$_x$, discharge through the model lateral boundary occurs, and when WTD falls below WTD$_x$ recharge into the modeled grid cells occurs (Figure 2). These lateral fluxes thus both determine and are determined by WTD, which in turn determines surface fluxes.

2.1.3. Vertical Water Fluxes

Vertical surface boundary influxes from *P* are provided as inputs to the model, as are incoming shortwave and longwave radiation, air temperature, humidity, and wind speed used to drive energy balance calculations. These calculations drive vertical surface boundary effluxes of ET from vascular canopy surfaces (E2–E3) and of evaporation (*E*) from nonvascular canopy (E2), residue (A6), and soil surfaces (A7). These effluxes are coupled with subsurface water transfers through root (F1–F6) and soil (B1–B5 and B18–B24) profiles within the modeled grid cells. Both lateral and vertical subsurface water flows through soil matrices within the modeled grid cells (B2) are calculated from the Richard's equation using total soil water potentials (ψ_s; matric + osmotic + gravimetric) of adjacent cells if both source and destination cells are either saturated or

D_{humm} (m)	D_{holl} (m)	ρ_b (Mg m⁻³)	$\theta_{v,fc}$ (m³ m⁻³)	$\theta_{v,wp}$ (m³ m⁻³)	$K_{s,mat}$ (mm h⁻¹)	θ_{mac} (m³ m⁻³)	ψ_{in} (MPa)	θ_r (m³ m⁻³)	n (-)	α (MPa⁻¹)
0.010		0.010	0.091	0.074		0.29	-0.0046	0.073	5.84	-211
0.065										
0.085		0.015	0.124	0.091		0.26	-0.0051	0.090	5.61	-189
0.115		0.020	0.157	0.102		0.22	-0.0056	0.100	5.51	-172
0.135		0.010	0.091	0.074		0.29	-0.0051	0.073	5.84	-211
0.190										
0.295										
0.305	0.005									
0.350	0.050	0.057	0.314	0.061	18.00	0.00	-0.0020	0.059	1.98	-350
0.540	0.240									
0.650	0.350									
0.720	0.420									
0.900	0.600	0.076	0.393	0.083		0.00	-0.0010	0.064	1.58	-529
1.100	0.800									
2.000	1.700									

Hummock surface

WTD$_x$ = 0.19 m (2003-2005)

WTD$_x$ = 0.35 m (2006-2007)

Lateral Discharge

Hollow surface

WTD$_x$ = 0.72 m (2008-2009)

L_t = 100 m

Lateral Recharge

Clay sediment with low permeability

Figure 2. Layout for *ecosys* model run to represent physical and hydrological characteristics of a Western Canadian fen peatland. Figure is not drawn to scale. D_{humm} = depth to the bottom of a layer from the hummock surface, D_{holl} = depth to the bottom of a layer from the hollow surface, ρ_b = dry bulk density [*Flanagan and Syed*, 2011], $\theta_{v,fc}$ = volumetric soil water content at field capacity (-0.01 MPa) and $\theta_{v,wp}$ = volumetric soil water content at wilting point (-1.5 MPa) [*Boelter*, 1969, 1970; *Päivänen*, 1973; *Szymanowski*, 1993], $K_{s,mat}$ = saturated hydraulic conductivity of soil matrix [*Boelter*, 1969], θ_{mac} = volumetric macropore fractions, WTD$_x$ = external reference water table depth representing average water table depth of the adjacent ecosystem, L_t = distance from modeled grid cells to the adjacent watershed over which lateral discharge/recharge occurs, ψ_{in} = matric water potential at the inflection point, θ_r = residual soil water content, and n and α = van Genuchten model (VGM) shape parameters.

unsaturated (B3) or from the Green-Ampt equation using ψ_s beyond the wetting front of the unsaturated cell if either cell is saturated (B4–B5) [*Grant et al.*, 2004]. Lateral and vertical subsurface water flows can also occur within the soil profiles through macropores using Hagen-Poiseuille's theory for laminar flow in tubes (B18–B21), depending on inputs for macropore volume fraction (B22) [*Dimitrov et al.*, 2010].

Vertical surface boundary effluxes from vascular T (E3) are governed by canopy conductance (g_c) ($=1/r_c$, where r_c = canopy stomatal resistance) determined by equilibrating plant water uptake (U_w), calculated from gradients of soil, root, and canopy water potentials (ψ_s, ψ_r, and ψ_c) regulated by soil and root hydraulic resistances (Ω_s and Ω_r) in each rooted soil layer, with T calculated from canopy energy exchange within a soil-plant-atmosphere continuum (F6). Since nonvascular plants lack stomatal regulation, E from nonvascular canopy is predominantly determined by vapor pressure gradient between the canopy and adjacent air (E3) and a specified fixed canopy surface resistance to E (E6). Nonvascular U_w is modeled similarly to the vascular canopy-root-soil hydraulic scheme.

Vascular root growth used to calculate Ω_s and Ω_r in each plant population is calculated from its assimilation of the nonstructural C product of CO_2 fixation (σ_C; G8). Assimilation is driven by growth respiration (R_g; G7) remaining after subtracting maintenance respiration (R_m; G6) from autotrophic respiration (R_a; G1) driven by oxidation of σ_C (G2–G5). This oxidation in roots may be limited by O_2 reduction (G3), required to sustain C oxidation and nutrient uptake (G5). O_2 reduction is driven by O_2 demand of roots and constrained by root O_2 uptake controlled by concentrations of aqueous O_2 in the soil ([O_{2s}]). Values of [O_{2s}] are maintained by convective-dispersive transport of O_2 through soil gaseous and aqueous phases (H3 and H5) and by dissolution of O_2 from soil gaseous to aqueous phases (H1). Vascular root O_2 uptake is also controlled by concentrations of aqueous O_2 in roots ([O_{2r}]; G4). Values of [O_{2r}] are maintained by convective-dispersive transport of O_2 through the root gaseous phase (H4) and by dissolution of O_2 from root gaseous to aqueous phases (H2). This transport depends on species-specific values used for root air-filled porosity (aerenchyma, θ_{pr}; H5). *Ecosys*, however, does not simulate nonvascular O_2 transport from atmosphere to rhizosphere, i.e., $\theta_{pr} = 0$ for mosses.

Slower production of σ_C in understorey nonvascular plants (e.g., mosses) is modeled in *ecosys* from interspecific competition for light and nutrients (N, P) with overstorey vascular plants and from intraspecific competition for those resources due to large moss population (G9). This slower σ_C production in the moss canopy

causes less aboveground to belowground transfer of σ_C and hence slower growth respiration (R_g; G7) and growth by individual moss plants. This in turn results in shallower moss belowground penetration. Absence of aerenchyma in moss hinders belowground O_2 uptake and hence oxidation of σ_C that further slows moss belowground R_g and growth in wet deeper peat layers, where $[O_{2s}]$ is inadequate for σ_C oxidation (G9–G10). This limits moss belowground biomasses mostly to near-surface peat layers that are infrequently saturated. Moss U_w in *ecosys* is thus solely dependent upon adequate vertical recharge of these near-surface shallow peat layers either from precipitation or through capillary rise from WT. When WTD deepens past a certain point, inadequate capillary rise causes near-surface peat desiccation (B2–B5), reducing ψ_s and increasing Ω_s (F3) of those layers. This in turn causes a reduction in moss canopy water potential (ψ_c) while equilibrating moss E with U_w (F6).

Deeper rooting by larger vascular plants in *ecosys*, on the other hand, is facilitated by greater root growth stimulated by greater assimilation and consequent rapid shoot-root transfer of σ_C due to more access to light and less intraspecific competition with lower population than mosses, as well as O_2 transfer through root aerenchyma into wet deeper peat layers (G2–G5, H2, and H4–H5). This deeper rooting pattern and consequent increased U_w from the wetter deeper layers enable those vascular plants to offset the suppression of U_w from desiccated near-surface layers. Those vascular plants can therefore limit the reduction in ψ_c and g_c and can sustain T (E3 and E6) during deeper WTD.

2.1.4. van Genuchten (VGM) Model Versus Modified Campbell Model (MCM) in Simulating Vertical and Lateral Water Fluxes

The rates of vertical and lateral fluxes through soil matrices in *ecosys* are governed by hydraulic gradients and unsaturated hydraulic conductivities in Richard's or Green-Ampt equations that are affected by soil matrix moisture retention. Soil matrix moisture retention in *ecosys* is currently simulated by log-transforming a Campbell equation (equation (1)) [*Campbell*, 1974] in two segments, one above field capacity and the other below (equations (3a,b) and (4a,b)) instead of using a parameter value for *b* representing peat soil texture as suggested by *Letts et al.* [2000] [*Frolking et al.*, 2002; *St-Hilaire et al.*, 2010].

$$\psi_m(\theta) = \psi' \left(\frac{\theta}{\theta_s} \right)^{-b} \tag{1}$$

Log-transforming equation (1) we had

$$\psi_m(\theta) = \exp\left[\ln(-\psi') + b(\ln\theta_s - \ln\theta) \right] \tag{2}$$

Splitting the curve derived from equation (2) into two subcurves at field capacity we had

$$\psi_m(\theta) = \exp\left[\ln(-\psi_{fc}) + b\left(\ln\theta_{v,fc} - \ln\theta\right)\right] (\text{if } \theta < \theta_{v,fc})$$
$$= \exp\left[\ln(-\psi') + b\left(\ln\theta_s - \ln\theta\right)\right] (\text{if } \theta \geq \theta_{v,fc}) \tag{3a,b}$$

In equations (3a,b), *b* was calculated as

$$b = \frac{\ln\left(-\psi_{wp}\right) - \ln(-\psi_{fc})}{\ln\theta_{v,fc} - \ln\theta_{v,wp}} (\text{if } \theta < \theta_{v,fc})$$
$$= \frac{\ln(-\psi_{fc}) - \ln(-\psi')}{\ln\theta_s - \ln\theta_{v,fc}} (\text{if } \theta \geq \theta_{v,fc}) \tag{4a,b}$$

where $\psi_m(\theta)$ = soil water matric potential (−MPa) as a function of θ, θ = ambient soil moisture content (m³ m⁻³), ψ' = soil water matric potential at saturation (−MPa), θ_s = soil moisture content at saturation (m³ m⁻³), *b* = dimensionless parameter representing influence of soil texture on slope of moisture retention curve, ψ_{fc} and $\theta_{v,fc}$ = soil water potential (−MPa) and soil moisture content (m³ m⁻³) at field capacity, and ψ_{wp} and $\theta_{v,wp}$ = soil water potential (−MPa) and soil moisture content (m³ m⁻³) at wilting point.

This modification of Campbell model (equations (3a,b) and (4a,b)) enabled *ecosys* to take advantage of available measurements of field capacity and wilting point that have physical meanings. Total porosity of a grid cell is calculated from dry bulk density (ρ_b) input and is used as θ_s for that grid cell. ψ_{fc} and ψ_{wp} are user defined ($\psi_{fc} = -0.01$ MPa and $\psi_{wp} = -1.5$ MPa for peat soils), and $\theta_{v,fc}$ and $\theta_{v,wp}$ are model inputs based on site measurements.

Simulation of peat moisture desorption by the MCM in *ecosys* has been tested only against the measurements from peat soils with low near-saturation moisture-holding capacity [*Dimitrov et al.*, 2010; *Mezbahuddin et al.*, 2015]. In those studies, the peat θ started dropping sharply right below ψ' and consequently were well modeled by the MCM in *ecosys*. However, MCM could underestimate θ of peats that retain high moisture near ψ' and rapidly drain below a threshold (i.e., air entry potential, ψ_e; Figure 1). The van Genuchten model (VGM) [*van Genuchten*, 1980] (equations (5) and (6)) can better model this type of retention by simulating higher θ near saturation, with sharp declines in ψ when ψ_m declines below ψ_e (Figure 1).

$$S_e = \frac{\theta - \theta_r}{\theta_s - \theta_r} \qquad (5)$$

$$\psi_m(\theta) = \frac{\left(S_e^{-\frac{1}{m}} - 1\right)^{\frac{1}{n}}}{\alpha}, \text{ where } m = 1 - 1/n \qquad (6)$$

where S_e = relative degree of saturation (Figure 1), θ_r = residual soil moisture content ($m^3\,m^{-3}$), n = van Genuchten parameter that describes the mean slope of the desorption curve or the range of pore size distribution, and α = equivalent to the inverse of the pressure head at ψ_e (i.e., $\alpha \approx 1$/air entry potential) that governs the shape of desorption curve ($-MPa^{-1}$).

A higher value of α in VGM (equation (6)) can simulate larger θ at a given ψ_m compared to MCM (Figure 1). However, an accompanying higher n value would also simulate rapid pore drainage once the ψ_m falls below the ψ_e (Figure 1). Values for the VGM parameters θ_r, n, and α (equations (5) and (6)) are usually derived from inverse optimization by using least squares method while fitting sets of measured θ and corresponding ψ_m [*van Genuchten et al.*, 1991]. However, substitution of MCM with VGM in *ecosys* requires use of a simpler method for parameter optimization to make use of the existing input structure of *ecosys* that only requires inputs for commonly measured soil physical and hydrologic parameters such as ρ_b (to calculate θ_s), $\theta_{v,fc}$, and $\theta_{v,wp}$. This simple parameter optimization in VGM simulation of *ecosys* is thus performed by solving B8–B15 using maximum of 19,000 iterations up to the point at which the squares of the differences between observed and simulated $\theta_{v,fc}$, and $\theta_{v,wp}$ approaches $\leq 10^{-6}$. To obtain a unique set of the VGM parameters from a particular optimization, an additional input for ψ_{in} (B10) for each soil layer is required (Figure 1). This ψ_{in} represents soil water matric potential at inflection point of the semilogarithmic VGM desorption curve and can be estimated from measured soil moisture retention curves (Figure 1). The inputs for ψ_{in} would affect the values of α in VGM curves (B10) and thus would govern the extent of moisture retention close to saturation. For instance, a lower ψ_{in} input would result in a higher α (B10) and a consequent lower ψ_e (since $\alpha \approx 1/\psi_e$) and hence a higher moisture retention at lower matric potentials and vice versa (Figure 1).

2.1.5. Snowpack and Freezing-Thawing

Snowpack hydrology and freeze-thaw dynamics of snowpack and underlying litters and peats are integral parts of northern boreal peatland water balances. *Ecosys* simulates snowpack as a single layer. Depth of the snowpack is calculated by dividing bulk volume of snow, water, and ice in the snowpack by the basal area of the snowpack (D5). The snow density (D5) increases over time with melting of snow to water and refreezing as ice (D6). The snowpack exchanges heat with the atmosphere (D1), underlying litters, and soil surface through conduction and vapor convection (D2 and D4). Snow meltwater directly infiltrates into surface litter layer and soil surface and can run off when the rate of snowmelt exceeds that of infiltration.

Freezing and thawing are calculated when snowpack, surface litter layer, or a soil layer temperature falls below or rise above the freezing point of the snowpack, surface litter layer, or that soil layer. Freezing point of the snowpack is considered the same as freezing point of free water, while for each soil and the surface litter layer, it is calculated from freezing point depression equation using ψ_s (D3). The rate of freezing or thawing is calculated from a 3-D general heat balance equation governed by bulk heat capacity, vertical and lateral heat fluxes, and the difference between ambient and freezing temperature of each of snowpack, surface litter, or soil layers (D2).

2.2. Modeling Experiment

2.2.1. Study Site

The ecohydrology algorithms in *ecosys* are tested in this study against measurements of peat water content, WTD, and ecosystem energy fluxes from 2003 to 2009 in a flux station of Fluxnet-Canada Research Network established at the WPL (latitude: 54.95°N, longitude: 112.47°W). The study site is a moderately nutrient-rich treed fen peatland within the Central Mixedwood Subregion of Boreal Alberta, Canada. Peat depth around

the flux station was about 2 m. This peatland is dominated by stunted trees of black spruce (*Picea mariana*) and tamarack (*Larix laricina*) with an average canopy height of 3 m. High abundance of a shrub species *Betula pumila* (dwarf birch) and the presence of a wide range of mosses, e.g., *Sphagnum* spp., feather moss, and brown moss, characterize the understorey vegetation of WPL. The topographic, climatic, edaphic, and vegetative characteristics of this site were described in more details by *Syed et al.* [2006].

2.2.2. Field Data Sets

Ecosys model inputs of half hourly weather variables, i.e., incoming shortwave and longwave radiation, air temperature, wind speed, precipitation, and relative humidity during 2003–2009, were measured at the micrometeorological station established at WPL [*Syed et al.*, 2006]. Ecosystem net radiation (R_n) was calculated by *Syed et al.* [2006] and *Flanagan and Syed* [2011] from measured incoming and outgoing shortwave and longwave radiation. Modeled outputs of hourly WTD and daily θ were tested against site-measured WTD (from average hummock surface) and θ (at 0.075, 0.1, and 0.125 m depths below hummock surface) to test adequacy of WTD and peat moisture retention simulation in *ecosys* [*Flanagan and Syed*, 2011]. Since snowpack hydrology is an important component of WPL water balance, modeled outputs of hourly snowpack depth were also tested against values of hourly measured snowpack depth. Snowpack depth was monitored by an acoustic distance sensor that was mounted above a sheet of plywood secured on the peat surface in an area away from trees. To examine how well *ecosys* simulated the surface energy exchange and hence vertical boundary water effluxes, hourly modeled latent heat (*LE*) and sensible heat (*H*) fluxes were tested against eddy covariance (EC) measurements of *LE* and *H* by *Syed et al.* [2006] and *Flanagan and Syed* [2011]. They also measured net ecosystem CO_2 fluxes by using EC micrometeorological approach. Erroneous EC *LE*, *H*, and CO_2 measurements due to stable air condition were screened out by using a friction velocity (u^*) of 0.15 m s^{-1} [*Syed et al.*, 2006]. The resultant data gaps were filled by extrapolation of valid measurements using moving windows of 15 day periods [*Wever et al.*, 2002; *Syed et al.*, 2006]. Net CO_2 fluxes were partitioned into gross primary productivity (GPP) and ecosystem respiration (R_e) by using Fluxnet-Canada Research Network standard protocol except for the application of an energy balance closure adjustment [*Syed et al.*, 2006]. More details about site measurements, screening, gap filling, and partitioning of EC fluxes can be found in *Wever et al.* [2002], *Syed et al.* [2006], and *Flanagan and Syed* [2011].

2.2.3. Model Runs

One model run for each of the MCM and VGM simulations of *ecosys* was set up. Each of these runs had a hummock and a hollow grid cell of 1 m × 1 m, which exchanged water, heat, carbon, and nutrients (N, P) (Figure 2). The hollow grid cell in each run had a near-surface peat layer that was 0.3 m thinner than the hummock cell representing a hummock-hollow surface difference of 0.3 m observed in the field (Figure 2) [*Long*, 2008]. Any depth with respect to the modeled hollow surface would thus be 0.3 m shallower than the depth with respect to the modeled hummock surface.

Dry bulk density (ρ_b) input for each soil layer was obtained from empirical relationships between ρ_b and peat depth in *Flanagan and Syed* [2011] constructed from measurements at the WPL (Figure 2). Input values for θ at field capacity ($\theta_{v,fc}$) and wilting point ($\theta_{v,wp}$) for each of the layers were derived from generalized empirical equations of $\theta_{v,fc}$ and $\theta_{v,wp}$ as functions of ρ_b developed by *Boelter* [1969, 1970], *Päivänen* [1973], and *Szymanowski* [1993] for northern boreal peatlands (Figure 2). Input values for matric potentials at inflection points (ψ_{in}) for the top 0.19 m of the VGM simulation were derived from moisture retention curves constructed by using θ measurements at corresponding depths of WPL and the height of those measurement depths above the WT (Figure 2). The ψ_{in} inputs for the remaining layers were derived from generalized moisture retention curves by *Boelter* [1969, 1970], *Päivänen* [1973], and *Szymanowski* [1993].

Due to the lack of pore size distribution measurements in WPL, we could not use measured values for macropore volume fractions (θ_{mac}) in the model. Instead, we used an analogy similar to that of *Silins and Rothwell* [1998] and *Wösten et al.* [2008], who calculated peat macroporosity as the fraction of total porosity drained at matric water potentials very close to saturation. This matric potential however varied from −0.0004 to −0.004 MPa in those studies depending upon peat types. Following their analogy, we assumed that the fraction of total porosity drained at a water potential of −0.003 MPa as θ_{mac} for a particular layer and used those values as model inputs (Figure 2). Higher moisture retention in the two layers 0.065–0.085 and 0.085–0.115 m compared to the layer below was indicated by soil moisture content measurements at depths corresponding to the midpoints of those layers. This was accordingly represented in our model runs by higher inputs of ρ_b, $\theta_{v,fc}$, and $\theta_{v,wp}$ and lower inputs of θ_{mac} in those two layers compared to the layer below (Figure 2).

Macropore saturated hydraulic conductivities in the model were calculated from the θ_{mac} inputs by using Hagen-Poiseuille's equation (B18–B22) [*Dimitrov et al.*, 2010]. Saturated hydraulic conductivities for the remaining soil matrices ($K_{s,mat}$) were given as model inputs (Figure 2). Since the soil matrix in our modeling represented the fraction of bulk soil excluding macropores, we used $K_{s,mat}$ values measured by *Boelter* [1969] for well-decomposed peat layers in a similar peatland. Lateral saturated hydraulic conductivity of the macropore and the soil matrix fraction of each layer were assumed to be equal to its macropore and soil matrix vertical saturated conductivities.

Each of the VGM and the MCM simulations of *ecosys* was run for a spin-up period of 1961–2002 under repeating 7 year sequences of hourly weather data (incoming shortwave and longwave radiation, air temperature, wind speed, humidity, and precipitation) recorded at the site from 2003 to 2009. Since site measurements stopped at the end of September in 2009, we filled October–December weather sequence in 2009 by those measured for the same period in 2008 to complete the 7 year weather sequences in spin-up runs. This spin-up period allowed energy and CO_2 exchanges in the model to achieve stable values through successive weather sequences.

Lateral water transfer between modeled grid cells in *ecosys* and the adjacent ecosystem occurs to and from a set external WTD (WTD_x). This WTD_x represents average watershed WTD with reference to average hummock surface, and it remains the same throughout the model run. This assumption was not valid for WPL site, since there was a drying trend observed from 2003 to 2009 due to diminishing precipitation [*Flanagan and Syed*, 2011] that caused WTD drawdown in the watershed in which WPL is located, which thereby increased the WTD of this fen peatland. To accommodate the gradual drying effects of catchment hydrology on modeled fen peatland WTD, we set the WTD_x at different levels based on the annual wetness of weather, e.g., shallow WTD_x for wetter years, intermediate WTD_x for regular years, and deep WTD_x for drier years (Figure 2). This scheme simulates larger hydraulic gradients between modeled WTD and the WTD_x for lateral recharge than discharge, resulting in net lateral water gains in wetter years and net losses in drier years (Figure 2). The WTD_x for the spin-up runs was thus set at 0.19, 0.35, and 0.72 m below the hummock surface (0.11 m above and 0.05 and 0.42 m below the hollow surface), following shallowest measured WTD in 2003–2005, average measured WTD in 2006–2007, and deepest measured WTD in 2008–2009 representing a gradual drying trend in overall watershed hydrology (Figure 2). L_t was set to a fixed 100 m in all directions for all years (Figure 2). The lower boundary condition in each of our model runs was defined; such that, there was no exchange of water to represent the presence of clay sediment with very low permeability underlying the peat [*Syed et al.*, 2006] (Figure 2). Although change in peat surface elevation with changing hydrology is an important component of hydrological self-regulation in northern peatlands [*Dise*, 2009], it is not represented in the current version of *ecosys*. Instead, we assumed a constant surface elevation for our modeled peatland in this study. However, we did not have any measurements in the site to examine if there was movement of peat surface over time, and if so, how much the movement was and how much uncertainty it could result due to the assumption of a constant surface in the modeling versus moving peat surface in the field.

At the beginning of the spin-up run, the hummock grid cells were seeded with evergreen needleleaf and deciduous needleleaf overstorey plant functional types (PFTs) to represent the black spruce and tamarack trees at the WPL. The modeled hollow grid cells were seeded only with the deciduous needleleaf overstorey PFT (to represent tamarack) since the black spruce at the site was found to grow only in the raised areas or hummocks. Each of the modeled hummock and the hollow was also seeded with a deciduous broadleaved vascular (to represent dwarf birch) and a nonvascular (to represent mosses) understorey PFTs. These PFTs are the same as those in earlier studies with *ecosys* in northern boreal ecosystems [*Grant et al.*, 2009, 2012; *Dimitrov et al.*, 2011]. The planting density was such that the population density of the evergreen needleleaf and the deciduous needleleaf PFT was 0.16 and 0.14 m^{-2} at the end of the spin-up run after accounting for annual mortality, thereby representing the site measured population of the two dominant overstorey species during the study period [*Syed et al.*, 2006]. The understorey deciduous broadleaved and the moss PFTs had population densities of 0.3 and 500 m^{-2} at the end of the spin-up run. To include wetland adaptation, we selected a value of 0.1 for root porosity (θ_{pr}) used in calculating root O_2 transport through aerenchyma (H6) in the two overstorey PFTs. A higher θ_{pr} value of 0.3 for the understorey vascular PFT was selected to simulate better wetland adaptation in the understorey vegetation at the WPL. These input values for vascular θ_{pr} fall within the range of root porosities (0.01–0.34) measured for various plants taken from northern

temperate and boreal bogs, fens, and reed swamps [*Cronk and Fennessy*, 2001]. The θ_{pr} in wetland adapted species can also vary with intensity of waterlogging [*Cronk and Fennessy*, 2001]. However, current version of *ecosys* used the set input for θ_{pr} to simulate O_2 transport from atmosphere to rhizosphere through roots which did not vary with intensity in waterlogging.

When the modeled ecosystem had attained dynamic energy and carbon equilibria at the end of the spin-up run, we continued the spin-up run from 2003 to 2009 for each of the MCM and VGM simulations of *ecosys* by using a real-time weather sequence. We tested our outputs from 2004 to 2009 of the simulation runs against the available site measurements of peat water contents, WTD, and energy exchange over those years.

2.2.4. Model Validation

Daily measured soil water contents at 0.075, 0.1, and 0.125 m depths were used to corroborate daily modeled MCM and VGM soil water content outputs from the layers whose midpoints corresponded to the measurement depths. Hourly modeled WTD was first averaged 50:50 over the modeled hummock and the modeled hollow for both MCM and VGM runs and then tested against the hourly measured WTD. Comparative model performance of MCM versus VGM was examined by comparing R^2 and root-mean-square error (RMSE) from regressions of modeled on measured and measured on modeled soil water contents and WTDs (with respect to the hollow surface), respectively. A higher R^2 and a lower RMSE would mean a better performance in simulating peat moisture desorption and WTD. Since soil moisture content and WTD data do not always follow a normal distribution, an additional analysis of comparative model performance was done based on an index of agreement (*d*) proposed for model performance comparison by *Willmott* [1981, 1982] and *Willmott and Wicks* [1980] (equation (7)).

$$d = 1 - \left[\frac{\sum_{i=1}^{n}(P_i - O_i)^2}{\sum_{i=1}^{n}(|P_i'| + |O_i'|)^2} \right]; \ 0 \leq d \leq 1; \ P_i' = P_i - \overline{O}; \ O_i' = O_i - \overline{O} \qquad (7)$$

where n = number of observations, P = predicted value, O = observed value, and $\bar{O}$ = mean of the observed values. The nearer the d value to 1 the better would be the model performance. The model that performs better between the two (MCM versus VGM) based on the above-mentioned modeled versus measured statistics of soil water contents and WTD would be used for further analyses in the course of the study. The outputs from the remaining run would not be used any further in this paper.

Hourly R_n, LE, and H fluxes modeled by the simulation (VGM or MCM) selected from the above test were averaged 50:50 over the hummock and the hollow and then regressed on hourly measured EC fluxes. Model performance in simulating those energy fluxes was evaluated from regression intercepts ($a \to 0$), slopes ($b \to 1$), coefficients of determination ($R^2 \to 1$), and root-mean-square errors (RMSE $\to 0$).

2.2.5. Analyses of Model Results

Model performance in simulating effects of WT deepening on surface drying of the northern boreal peatland at WPL was evaluated by comparing modeled and measured Bowen ratios (β) (=H/LE). To examine the short-term effects on WTD drawdown on β, hourly modeled versus half hourly measured midday (2 h before and after solar noon, i.e., 17:00–21:00 local time) β was compared for three hydroperiods of 3 days each with gradually deeper WTD. These hydroperiods were chosen in mid-August of 2005, 2008, and 2009 on the basis of comparable weather conditions, i.e., R_n and vapor pressure deficit (*D*) in similar days and therefore distinguished from each other predominantly by the WTD. To further examine the consistency of the short-term effects of WTD drawdown on β over longer time scales, we also studied the effects of WTD drawdown on average β over late (mid-July to mid-August) and whole (May–August) growing seasons. Since atmospheric drivers like R_n and D can also affect β we therefore had to control for the effects of R_n and D in examining the net effects of WTD on β. To control for R_n effects on β, only the midday βs that were measured and modeled under clear-sky condition, i.e., incoming solar radiation >700 W m^{-2}, were selected and averaged over the late and/or whole growing seasons. Effects of *D* on β were screened out by selecting three *D* classes for both late (e.g., $D = 0.8$–1, 1–1.2, and 1.2–1.4 kPa) and the whole growing season (e.g., $D = 1$–1.5, 1.5–2, and 2–2.5 kPa) and by studying WTD effects on average β in each of those three *D* classes. The consistency of WTD effects on β in each of those *D* classes would further ensure the consistency of WTD effects irrespective of the effects of *D* on late and/or whole growing season β. Those *D* classes were selected on the basis of the
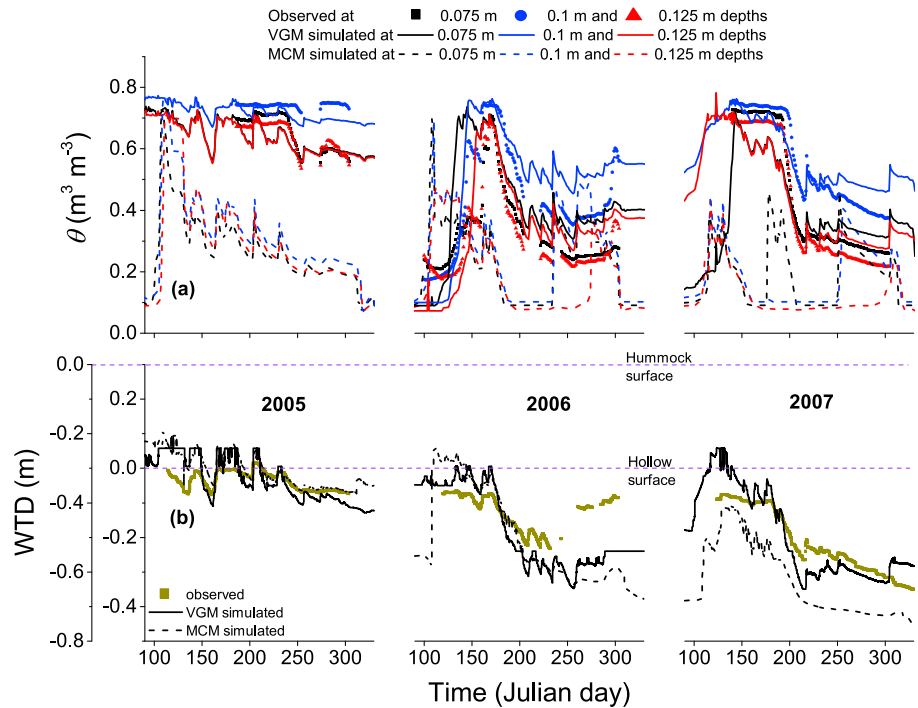
Figure 3. (a) Daily soil water contents (θ) simulated with *ecosys* using van Genuchten model (VGM) and modified Campbell model (MCM) and measured θ at 0.075, 0.1, and 0.125 m depths [*Syed et al.*, 2006; *Cai et al.*, 2010; *Long et al.*, 2010; *Flanagan and Syed*, 2011] from the hummock surface and (b) hourly water table depth (WTD) simulated with *ecosys* using VGM and MCM and measured half hourly WTD [*Syed et al.*, 2006; *Cai et al.*, 2010; *Long et al.*, 2010; *Flanagan and Syed*, 2011] during March–November 2005–2007 at a Western Canadian fen peatland. A negative WTD represents a depth below hummock/hollow surface, and a positive WTD represents a depth above hummock/hollow surface.

highest availability of measurements across *D* classes over the specified period (e.g., late or whole growing season) throughout 2004–2009.

In *ecosys* complete energy balance closure is achieved while solving for canopy, soil, residue, and snow surface temperature (D1 and E1), following energy and mass conservation theory, whereas in the EC measurements, ecosystem energy fluxes, e.g., *LE* and *H*, can be underestimated due to the lack of adequate convection and hence can yield incomplete energy balance closure [*Wilson et al.*, 2002]. This difference in energy balance closure between the modeled outputs and the EC measurements can also contribute to the divergence between modeled and measured WTD effects on β. To examine this divergence we compared modeled versus EC measured energy balance closure for each year from 2004 to 2009. This energy balance closure was calculated as the slope of regression of hourly $H + LE$ on hourly R_n-G (ground heat flux) for both modeled and EC measured ($u^* > 0.15\,\mathrm{m\,s^{-1}}$) energy fluxes. Since *G* was not measured in the field we assumed hourly *G* as 10% of hourly R_n as suggested by *Kellner* [2001].

Increases in GPP and ET across Canadian peatlands have been found to be closely associated with each other; i.e., increases in GPP were positively correlated to increases in ET [*Brümmer et al.*, 2012]. We thus compared modeled and measured water use efficiencies (WUEs) calculated from modeled and EC-derived GPP and ET (equation (8)) to further evaluate agreement or disagreement between modeled versus measured ET.

$$\mathrm{WUE_{modeled}} = \frac{\mathrm{GPP_{modeled}}}{\mathrm{ET_{modeled}}}; \mathrm{WUE_{EC\ gap\ filled}} = \frac{\mathrm{GPP_{partitioned}}}{\mathrm{ET_{EC\ gap\ filled}}} \qquad (8)$$

where $\mathrm{WUE_{modeled}}$ and $\mathrm{WUE_{EC\ gap\ filled}}$ = modeled and EC gap-filled WUE (g C kg^{-1} H$_2$O), $\mathrm{GPP_{modeled}}$ and $\mathrm{GPP_{partitioned}}$ = modeled GPP and partitioned GPP derived from EC gap-filled net CO$_2$ fluxes (g C m^{-2} h^{-1}) [*Syed et al.*, 2006], and $\mathrm{ET_{modeled}}$ and $\mathrm{ET_{EC\ gap\ filled}}$ = ET calculated from modeled and EC gap-filled *LE* fluxes (kg H$_2$O m^{-2} h^{-1}).
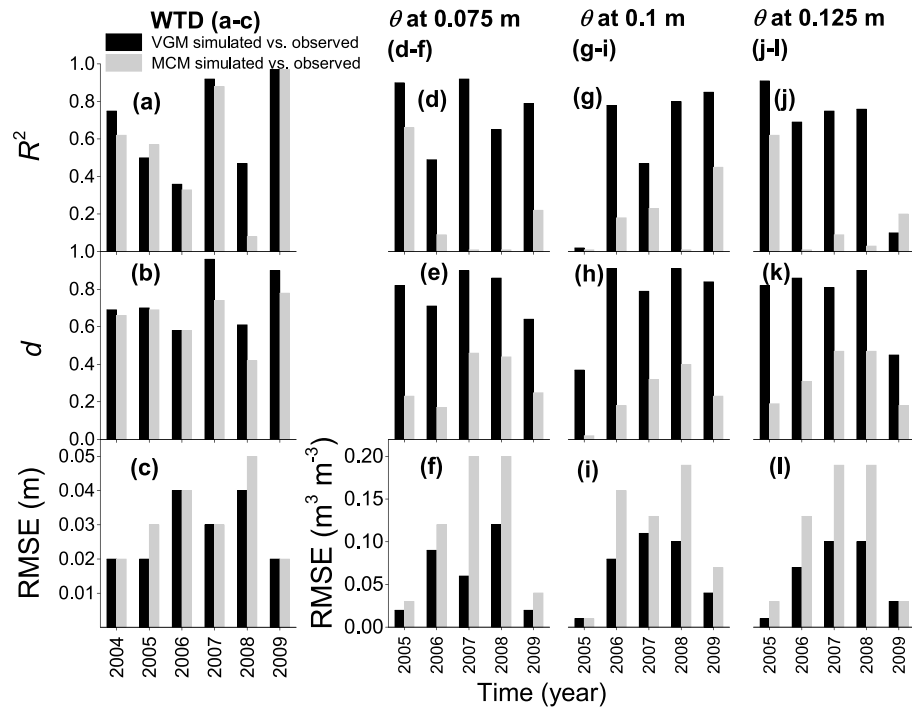
Figure 4. (a, d, g, and j) Coefficients of determination (R^2) from regressions of modeled on measured; (b, e, h, and k) index of agreement (d; section 2.2.5) between modeled and measured; and (c, f, i, and l) root-mean-square errors (RMSEs) from regressions of measured on modeled hourly water table depth (WTD) from hollow surface and daily soil water contents (θ) at 0.075, 0.1, and 0.125 m depths below the hummock surface, respectively, during 2004–2009 at a Western Canadian fen peatland.

3. Results

3.1. Peat Moisture Retention Simulation by van Genuchten Model (VGM) Versus Modified Campbell (MCM) Model

The VGM simulation of *ecosys* simulated peat θ better at 0.075, 0.1, and 0.125 m depths below the hummock surface at the WPL than did the MCM simulation (Figure 3a). This was apparent in higher modeled versus measured R^2 (Figures 4d, 4g, and 4j) and d (Figures 4e, 4h, and 4k) and lower measured versus modeled root-mean-square errors (RMSEs; Figures 4f, 4i, and 4l) in the VGM than in the MCM simulation of θ at all depths in all years. Despite this large divergence in θ simulations, both VGM and MCM simulations simulated the measured WTD at WPL almost equally well (Figure 3b). This was apparent in little difference in modeled versus measured R^2 (Figure 4a) and d (Figure 4b) and measured versus modeled RMSE (Figure 4c) between the VGM and the MCM simulations of *ecosys* for WTD in all years.

The improved simulation of peat θ by the VGM simulation of *ecosys* was achieved by computing higher moisture retention compared to the MCM simulation when θ was close to θ_s above the WT. For instance, VGM simulated θ at 0.075, 0.1, and 0.125 m depths below the hummock surface at the onset of springs in 2005–2007 which were very close to the measured θ and $>0.5\,m^3\,m^{-3}$ higher than the MCM simulated θ at the same depths when both the modeled and measured WTD was within 0.1 m below the hollow surface (within 0.4 m below the hummock surface; Figure 3a). However, at the end of May in 2006, when WTD fell below 0.1 m from the hollow surface (deeper than 0.4 m bellow the hummock surface), VGM simulated a gradual drop in θ at all three depths that corresponded well with the measurements (Figures 3a and 3b). The drop in θ with the similar drop in WTD simulated by MCM occurred from a much lower initial θ and about a month earlier than the measured (Figures 3a and 3b). During 2007 measured θ remained close to $0.7\,m^3\,m^{-3}$ until the end of June when WTD fell below 0.1 m from the hollow surface (Figures 3a and 3b). This trend was well captured by VGM but was completely missed by MCM (Figures 3a and 3b). Much earlier and more rapid drainage of peat pore in MCM during 2007 yielded more rapid discharge and hence deeper WTD compared to the measurements (Figure 3b). This trend of greater modeled versus measured WTD
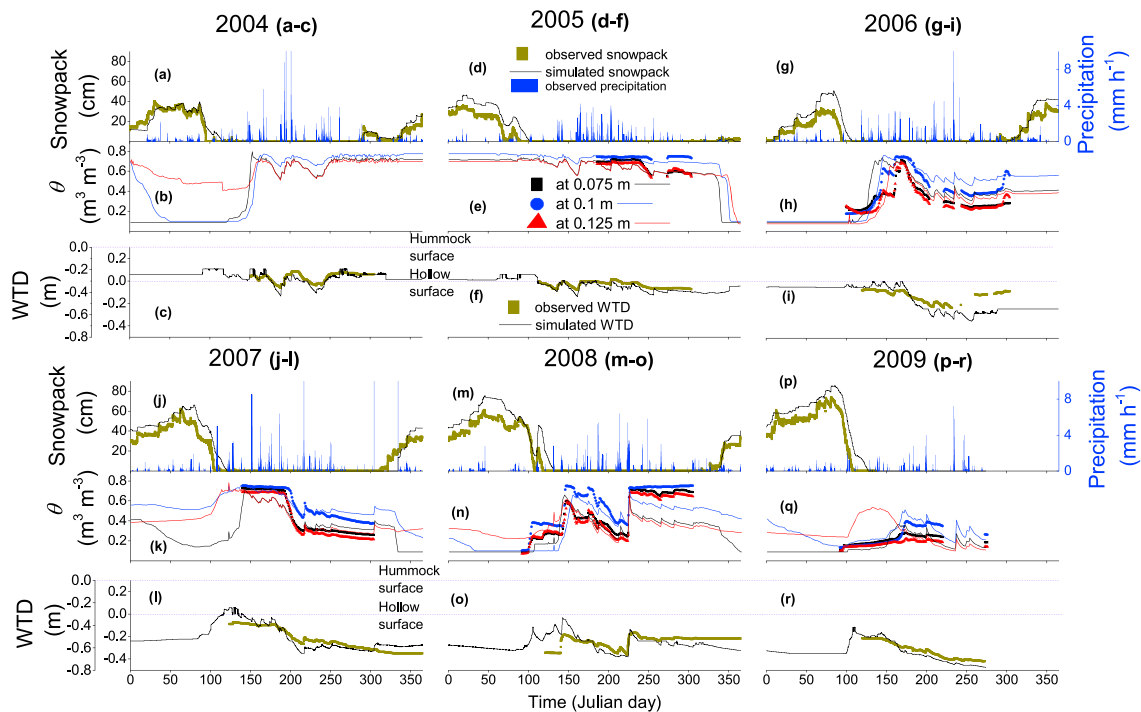
Figure 5. (a, d, g, j, m, and p) Half hourly measured and hourly modeled snowpack depth (on the left y axes) [*Syed et al.*, 2006; *Flanagan and Syed*, 2011] and half hourly measured precipitation (on the right y axes); (b, e, h, k, n, and q) daily modeled and measured soil water contents (θ) at 0.075, 0.1, and 0.125 m depths [*Syed et al.*, 2006; *Cai et al.*, 2010; *Long et al.*, 2010; *Flanagan and Syed*, 2011] below the hummock surface; and (c, f, i, l, o, and r) half hourly measured and hourly modeled water table depth (WTD) [*Syed et al.*, 2006; *Cai et al.*, 2010; *Long et al.*, 2010; *Flanagan and Syed*, 2011] from 2004 to 2009 at a Western Canadian fen peatland. A negative WTD represents a depth below hummock/hollow surface, and a positive WTD represents a depth above hummock/hollow surface.

divergence in the MCM simulation also continued in 2008 and 2009 as apparent in lower MCM modeled versus measured d compared to VGM (Figure 4b).

Since VGM simulation in *ecosys* substantially improved θ modeling than in MCM simulation, we hereafter use the outputs from VGM simulation of *ecosys* to test the rest of the hypotheses in this study.

3.2. Seasonal and Interannual Variations in Modeled Versus Measured WTD and θ

Seasonal and interannual variations in WTD measured at the WPL were modeled by *ecosys* from the balance between vertical and lateral water influxes (P and lateral recharge) and effluxes (ET and lateral discharge). During the growing season (May–August) of 2004, P frequently exceeded ET, resulting in a modeled WT that remained above the hollow surface for most of the growing season (Figures 5c and 6). This trend was also apparent in the site-measured WTD and the cumulative difference between P and EC gap-filled ET (P-ET$_{EC}$ gap filled; Figures 5c and 6). The shallow WTD was sustained by a shallow WTD$_x$ (=0.19 m; Figure 2) that created a hydraulic gradient that simulated net recharge during 2004 (Figure 7c), which stabilized the modeled WTD at the shallowest position in 2004 compared to that of 2005–2009 (Figures 5c, 5f, 5i, 5l, 5o, 5r, and 7a). This shallow WTD also enabled *ecosys* to simulate higher near-surface θ ($>0.5\,\text{m}^3\,\text{m}^{-3}$) at 0.075, 0.1, and 0.125 m depths below the hummock surface throughout the growing season of 2004 (Figure 5b). Short-term drops in P to ET ratio during late June–early July and late August resulted in a transient fall of modeled WTD below the hollow surface that was apparent in WTD measurements (Figures 5a and 5c). This transient drop of WTD caused a short-term drop in near-surface modeled θ (Figures 5b and 5c).

The WTD$_x$ (=0.19 m) in 2005 was set the same as that in 2004 (Figure 2). However, a lower P and a consequently lower P to ET ratio during the growing season of 2005 caused *ecosys* to simulate a slightly deeper growing season WTD than in 2004 (Figures 5c, 5f, 6, 7a, and 7b). This trend was also apparent in WTD measurements and the cumulative P-ET$_{EC}$ gap filled at the WPL (Figures 5f, 6, and 7a). A deeper modeled WTD with respect to WTD$_x$ in 2005 than in 2004 caused a larger hydraulic gradient that simulated more rapid lateral recharge in 2005 than in 2004 (Figures 2, 5c, 5f, and 7c). This more rapid lateral recharge in 2005 caused
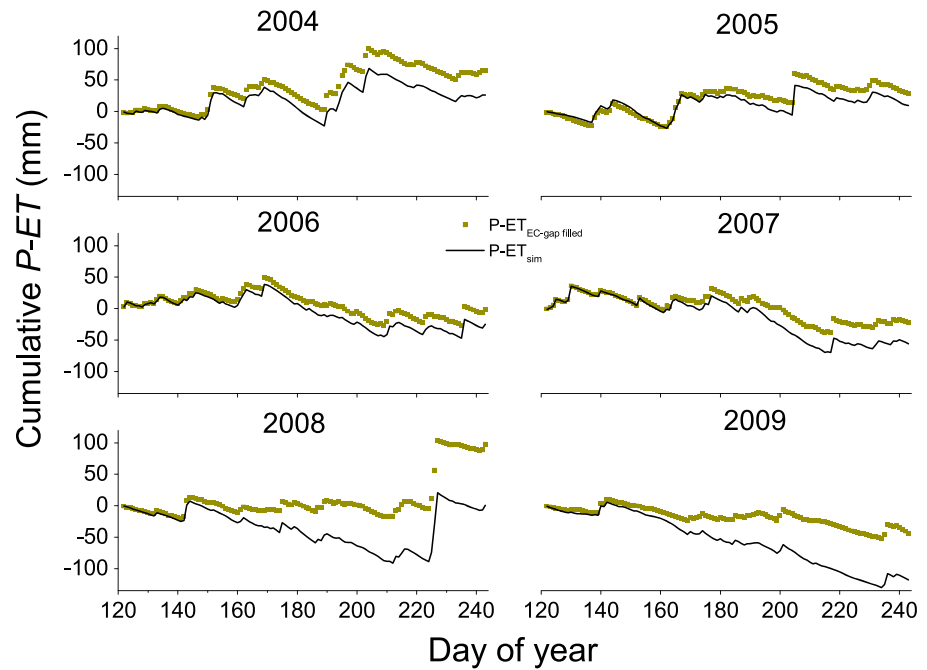
Figure 6. Cumulative differences between observed precipitation (*P*) and eddy covariance (EC) gap-filled evapotranspiration (ET) (*P*-ET$_{EC\ gap\ filled}$) [*Syed et al.*, 2006; *Flanagan and Syed*, 2011] and between observed *P* and simulated ET (*P*-ET$_{sim}$) during 2004–2009 at a Western Canadian fen peatland.

WTD to remain less than 0.1 m below the hollow surface, which enabled the modeled near-surface peats to retain high θ that was well corroborated by the measurements (Figure 5e).

The WTD$_x$ in 2006 (=0.35 m) was deeper than that in 2005 and 2004 (=0.19 m) (Figure 2), which created a smaller hydraulic gradient between modeled WTD and WTD$_x$ in 2006 that generated less recharge
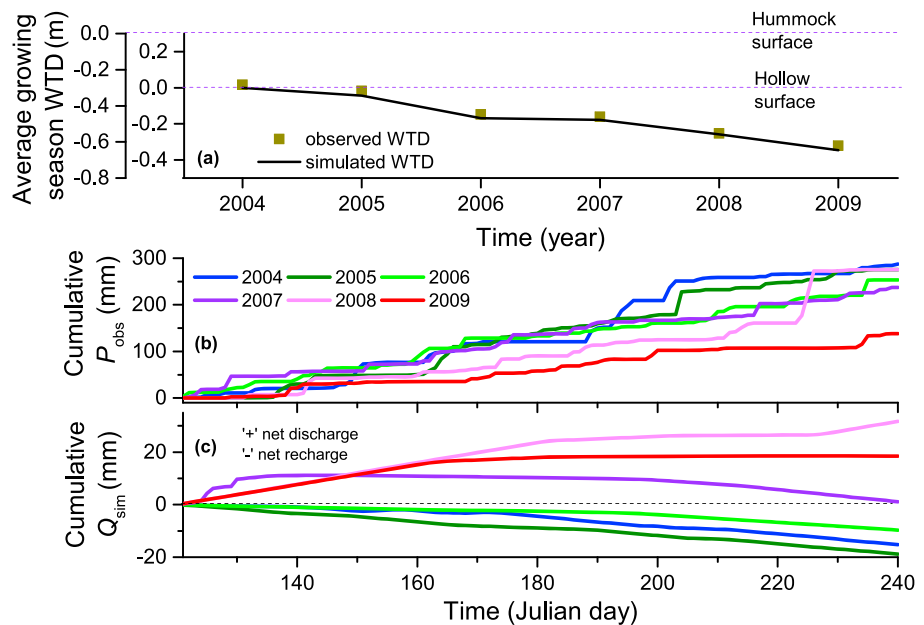
Figure 7. (a) Modeled and measured average water table depth (WTD), (b) cumulative observed precipitation (*P*$_{obs}$) [*Syed et al.*, 2006; *Flanagan and Syed*, 2011], and (c) simulated cumulative lateral recharge/discharge (*Q*$_{sim}$) over the growing season (May–August) of 2004–2009 at a Western Canadian fen peatland. A negative WTD represents a depth below hummock/hollow surface, and a positive WTD represents a depth above hummock/hollow surface.

(Figures 5i, 7a, and 7c). Less recharge along with declining P to ET ratio caused a gradual drawdown of WTD from early June to August in 2006 that in turn caused modeled θ to gradually fall from ~0.7 to ~0.45 $m^3\,m^{-3}$ at 0.1 m depth and from ~0.7 to 0.3 $m^3\,m^{-3}$ at 0.075 and 0.125 m depths (Figure 5h). This modeled trend of gradual WTD drawdown and the declines in near-surface θ due to reduction in P to ET ratio was also apparent in WTD, θ, and P-ET$_{EC\ gap\ filled}$ measured at the WPL (Figures 5i and 6). Smaller P to ET ratio along with less recharge during the growing season of 2006 stabilized modeled WTD in the growing season of 2006 at a deeper position than in 2005 (Figures 5i, 6, and 7a–7c).

The WTD$_x$ (=0.35 m) in 2007 was the same as that in 2006 (Figure 2). However, P in excess of ET during May 2007 caused modeled WTD to rise above WTD$_x$, creating a hydraulic gradient which generated lateral discharge and eventually stabilized modeled WTD at a position where the residual between P and ET equilibrated with the discharge (Figures 2, 5l, 6, and 7c). This early growing season discharge in 2007, however, ceased by the end of May when ET exceeded P and the modeled WTD gradually receded thereafter and consequently WTD fell below WTD$_x$ causing a hydraulic gradient that simulated lateral recharge (Figures 2, 5l, and 7c). This gradual decline in modeled WTD also caused a gradual decline in near-surface θ from late May to the end of the year (Figure 5k). This gradual decline in WTD and hence near-surface θ in 2007 was similar to that in 2006, but unlike in 2006 it did not start until late June in 2007 due to higher May–June precipitation in 2007 than in 2006 (Figures 5g–5i in 2006 versus Figures 5j–5l in 2007). This modeled interannual variation between 2006 and 2007 in declines of WTD and θ was also well corroborated by site measurements (Figure 5).

The WTD$_x$ in 2008 (=0.72 m) was deeper than that in 2007 (=0.35 m) (Figure 2). This was deeper than the modeled WTD during April–June in 2008 and generated a hydraulic gradient that drove a larger lateral discharge than in 2007 (Figures 2, 5o, and 7c). This lateral discharge caused a gradual drawdown of WTD from late May to July in 2008, which in turn caused a gradual decline in near-surface θ (Figure 5n). This lateral discharge, however, ceased as growing season progressed (Figure 7c). Larger lateral discharge and lower P to ET ratio stabilized the modeled WTD at a deeper position in the growing season of 2008 than in 2007 (Figures 5o in 2008 versus 5k in 2007, 6, 7a, and 7c). A large rainfall event in mid-August caused the near-surface θ to increase by almost twofold, which was modeled reasonably well by *ecosys* (Figure 5n). This rainfall event also caused a rise in both modeled and measured WTs (Figure 5o). Although the modeled seasonal trend in WTD and θ in 2008 was corroborated well by the measured WTD and θ, cumulative P-ET$_{EC\ gap\ filled}$ diverged from the cumulative difference between P and modeled ET (P-ET$_{sim}$) (Figures 5n, 5o, and 6).

The WTD$_x$ (=0.72 m) in 2009 was same as in 2008 (Figure 2). During the early growing season (April–May) in 2009, a modeled WTD was less than WTD$_x$, causing a hydraulic gradient that drove lateral discharge (Figure 7c). This lateral water loss through discharge caused *ecosys* to simulate the lowest early growing season near-surface θ during 2009 as measured at the WPL (Figure 5q). This lateral discharge in the model, however, ceased when modeled WTD fell below the WTD$_x$ as dry season progressed and then the resultant hydraulic gradient drove lateral recharge (Figures 2, 5r, and 7c). Besides, further reduction in P and a consequent reduction in P to ET ratio during the growing season of 2009 caused the modeled WTD to stabilize at a deeper position than in 2008, where the difference between ET and P was in equilibrium with the lateral recharge (Figures 5p, 5r, 6, 7a, and 7b). This modeled trend was well corroborated by the measured growing season WTD in 2009 versus 2008 at the WPL (Figures 5o versus 5r and 7a). However, like in 2008, P-ET$_{sim}$ in 2009 also significantly diverged from P-ET$_{EC\ gap\ filled}$ (Figure 6).

3.3. Sensitivity of Modeled WTD to Lateral Boundary Condition

The rates of the lateral water exchange in *ecosys* were largely affected by the hydraulic gradients between the modeled WTD and the WTD$_x$ (B23). The inputs of WTD$_x$ in the model thus affected the rates of modeled lateral water exchange and hence the seasonal and interannual variations in modeled WTD. To test the adequacy of these WTD$_x$ inputs in the current simulation, we performed three other runs by inputting constant WTD$_x$ of 0.19, 0.35, and 0.72 m from the hummock surface for all years instead of using these WTD$_x$ in different years as in the current run. A constant WTD$_x$ of 0.19 m created hydraulic gradients that generated larger lateral recharge and smaller lateral discharge than the current simulation and hence modeled shallower WTD than measured for the growing seasons of 2006 to 2009. A constant WTD$_x$ of 0.35 m simulated less recharge than the current simulation in 2004 and 2005 and hence modeled deeper WTD than the measured in those

Table 1. Statistics From Modeled Versus Measured Regressions of Ecosystem Energy Fluxes at a Western Canadian Fen Peatland[a]

| Year	2004	2005	2006	2007	2008	2009
Modeled versus observed ecosystem net radiation (R_n)						
n	8704	8752	8758	8752	8758	6872
a	10	10	8	10	8	10
b	0.97	0.96	0.96	0.95	0.95	0.96
R^2	0.99	0.99	0.99	0.99	0.99	0.99
RMSE (Wm^{-2})	10	15	17	17	17	19
Modeled versus eddy covariance (EC) measured ($u^* > 0.15\,\mathrm{m\,s^{-1}}$) ecosystem latent heat fluxes (LE)						
n	7142	5983	6033	6075	6789	3886
a	−3	−2	−3	−4	−2	−2
b	1.06	1.05	1.06	1.04	1.46	1.41
R^2	0.92	0.9	0.9	0.86	0.90	0.91
RMSE (Wm^{-2})	14	18	20	23	14	13
RMSRE (Wm^{-2})	14	14	15	15	12	12
Modeled versus EC measured ($u^* > 0.15\,\mathrm{m\,s^{-1}}$) ecosystem sensible heat fluxes (H)						
n	7143	5978	6031	6026	6135	3686
a	−11	−16	−14	−17	−14	−11
b	1.17	1.17	1.10	1.19	1.23	1.21
R^2	0.85	0.85	0.82	0.82	0.81	0.84
RMSE (Wm^{-2})	25	29	31	29	31	31
RMSRE (Wm^{-2})	12	12	12	12	12	12
Energy balance closure [slopes of regressions of $H + LE$ fluxes over R_n-G (ground heat flux)]						
EC gap filled	0.77	0.77	0.78	0.75	0.66	0.64
Modeled	1.00	1.00	1.00	1.00	1.00	1.00

[a]a and b are from simple linear regressions of modeled on measured. R^2 = coefficient of determination and RMSE = root mean square for errors from simple linear regressions of measured on simulated. RMSRE = root mean square for random errors in EC measurements calculated by inputting EC LE and H fluxes recorded at u^* (friction velocity) $> 0.15\,\mathrm{m\,s^{-1}}$ into algorithms for estimation of random errors in EC LE and H measurements developed for forests by *Richardson et al.* [2006]. Since G was not measured, we assumed hourly G as 10% of hourly R_n in calculating energy balance closure (section 2.2.5) [*Kellner*, 2001].

years. This also simulated smaller discharge and larger recharge than the current simulation in 2008 and 2009 and hence modeled shallower WTD than the measured for the growing seasons in those years. A constant WTD$_x$ of 0.72 m simulated greater lateral discharge and hence modeled deeper WTD than the measured for the growing seasons of 2004 to 2007. Thus, accurate modeling of WTD required changes in WTD$_x$ during the model run.

Like WTD$_x$, inputs for L_t also governed the rates of lateral water recharge and discharge and hence the variations in modeled WTD. To test the adequacy of the input for L_t in our current simulation, we performed two other runs by inputting 10 m and 200 m in all directions instead of 100 m in the current simulation run leaving everything else unchanged. L_t = 10 m in all directions simulated faster lateral discharge/recharge than the current model run and hence smaller seasonal fluctuations in WTD than measured. L_t = 200 m simulated slower lateral discharge/recharge than the current model run and hence larger seasonal fluctuations in WTD than measured. Therefore, these sensitivity tests suggested that, for the given input of saturated hydraulic conductivity of each peat layer, the lateral boundary condition defined by the combination of inputs for WTD$_x$ (0.19 m for 2004–2005, 0.35 m for 2006–2007, and 0.72 m for 2008–2009) and L_t (100 m in all directions) in our current simulation best simulated the balance between lateral recharge and discharge and hence the seasonal and interannual variations in WTD as measured at the WPL.

3.4. Modeled Versus Measured Snowpack and Freeze-Thaw

The depth and the timing of snowpack accumulation and soil freezing-thawing were also important components of hydrology in seasonally frozen peats at the WPL. Measured snowpack depth throughout the winter, timing of snowmelt during the spring, and the initiation of the snowpack accumulation at the onset of winter were simulated well by *ecosys* throughout the study period (Figures 5a, 5d, 5g, 5j, 5m, and 5p). However, the modeled snowpack depth was about 0.1 m thicker than the measured during January–March of 2005–2009 (Figures 5a, 5d, 5g, 5j, 5m, and 5p). The disappearance of the snowpack in the model was on an average
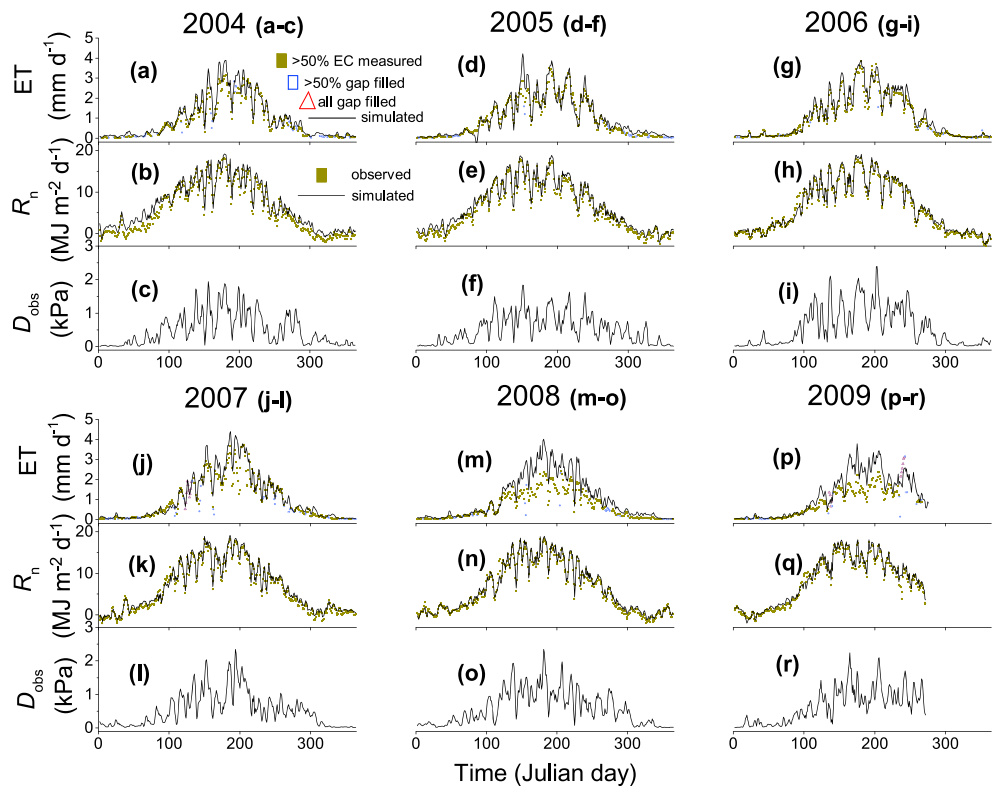
Figure 8. Three-day moving averages for (a, d, g, j, m, and p) eddy covariance (EC) gap-filled [*Syed et al.*, 2006; *Flanagan and Syed*, 2011] and modeled evapotranspiration (ET), (b, e, h, k, n, and q) observed and modeled net radiation (R_n), and (c, f, i, l, o, and r) observed vapor pressure deficit (D_{obs}) [*Syed et al.*, 2006; *Flanagan and Syed*, 2011] during 2004–2009 at a Western Canadian fen peatland.

10 days later than that measured (Figures 5a, 5d, 5g, 5j, 5m, and 5p). *Ecosys* simulates the effects of vegetation on the transfers of shortwave and longwave radiation to and from snow, litter, and soil surfaces and thereby their effects on snowmelt. These effects could delay snowmelt under canopies in relation to that in open areas. The snowpack depth was monitored only in an open area away from trees. However, *ecosys* did not distinguish between snowpack under tree canopies and in open areas. The black spruce canopy in the model intercepted radiation and hence reduced available energy for absorption by the modeled snowpack from that by the measured snowpack, which was away from the trees. Moreover, possible reduction in snowpack albedo due to fallen litters on top of snowpack was not accounted for in the model. These may explain the delayed disappearance of snowpack in the model versus in the measurements. Besides, changes in snowpack depth by erosion or accumulation due to wind and/or topography (ridge versus depressions) was not modeled at the time of this study. These changes may also explain some of the differences between modeled and measured snowpack depths. However, the timing and rates of thawing in near-surface peats was modeled reasonably well by *ecosys* as corroborated by measured θ during thawing periods of 2006, 2008, and 2009 (Figures 5h, 5n, and 5q).

3.5. Modeled Versus Measured Ecosystem Energy Fluxes

Ecosystem energy fluxes (R_n, LE, and H) control vertical water exchange between the ecosystem and the atmosphere. Agreement between modeled and measured energy fluxes thus indicated adequate simulation of drying effects on ET as WT receded. *Ecosys* simulated the diurnal and seasonal variations in ecosystem surface energy fluxes reasonably well. Regressions of hourly modeled versus measured R_n, LE, and H gave intercepts within 20 W m^{-2} of zero, and slopes within 0.1 of one, indicating minimal bias in modeled values for all years of the study except in 2008 and 2009 when LE was overestimated (Table 1). Larger values for R^2 (>0.8) and smaller values for RMSEs (~20 W m^{-2}) further indicated that *ecosys* simulated the diurnal and seasonal variations in energy fluxes reasonably well at the WPL (Table 1). Much of the unexplained variance in EC LE
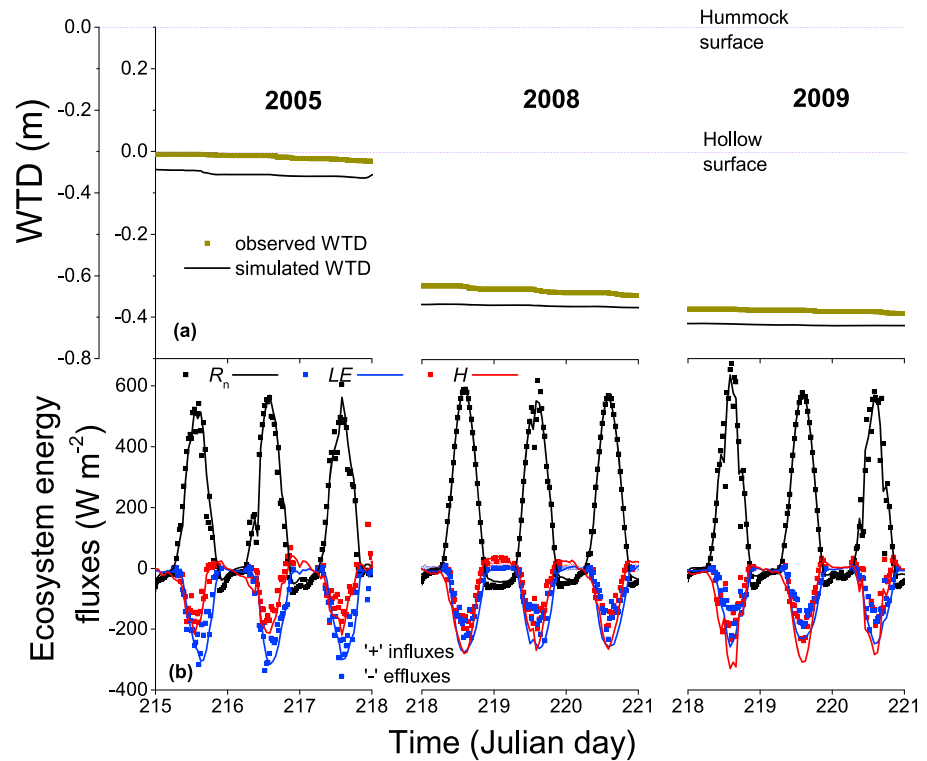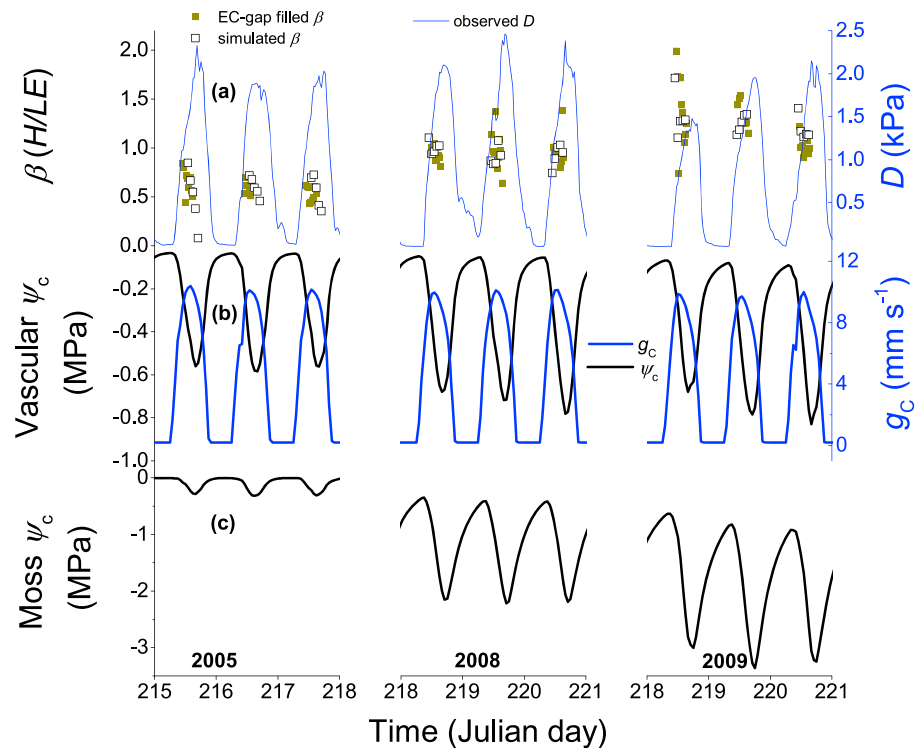
Figure 9. (a) Half hourly measured and hourly modeled water table depth (WTD) and (b) half hourly eddy covariance (EC) measured (u^* (friction velocity) $> 0.15\,\mathrm{m\,s}^{-1}$) [*Syed et al.*, 2006; *Flanagan and Syed*, 2011] and hourly modeled ecosystem energy fluxes (R_n = net radiation, LE = latent heat, and H = sensible heat flux) during August 2005, 2008, and 2009 at a Western Canadian fen peatland. The positive values for fluxes represent downward fluxes or fluxes into the ecosystem, and the negative values for fluxes represent upward fluxes or fluxes out of the ecosystem. A negative WTD represents a depth below hummock/hollow surface, and a positive WTD represents a depth above hummock/hollow surface.

and H could be attributed to a random error of approximately 20% in EC methodology [*Wesely and Hart*, 1985]. This attribution was corroborated by root mean squares for random error (RMSRE) in EC measurements over forests calculated from *Richardson et al.* [2006] that were similar to RMSE, indicating that further constraint in model testing could not be achieved without further precision in EC measurements. Modeled versus measured ecosystem energy flux divergence may also have been affected by incomplete energy balance closures of about 75% in the EC measurements for 2004–2007 and about 65% for 2008–2009 as opposed to complete energy balance closure in the model (Table 1).

3.6. Seasonal Variation in Modeled Versus Measured Surface Energy Exchange

The WPL ecosystem experienced strong seasonality in temperature and radiation that affected the seasonality in surface energy exchange. EC gap-filled daily ET gradually rose from the onset of the spring to the end of summer with the increase in temperature and hence vapor pressure deficit (D) and R_n before it gradually started falling off in the fall with declining D and R_n from 2004 to 2009 (Figure 8). *Ecosys* simulated this seasonality in ET reasonably well as suggested by modeled versus EC gap-filled daily ET from 2004 to 2009 (Figures 8a, 8d, 8g, 8j, 8m, and 8p). This seasonality in *ecosys* was modeled by adequately simulating (1) D from the inputs of air temperature and humidity (Figures 8c, 8f, 8i, 8l, 8o, and 8r) and (2) R_n (Figures 8b, 8e, 8h, 8k, 8n, and 8q) from the inputs of incoming solar radiation and by calculating radiation interception, absorption, and reflection by and from vegetation, litter, and peat surfaces. R_n at the vegetation surface was simulated from adequate modeling of seasonality in leaf area index (LAI) for the evergreen and the deciduous PFTs. This simulation was further corroborated by reasonable agreement between modeled versus measured peak LAI during July 2004, the only year in which measurements were carried out. Modeled peak LAI of $2.43\,\mathrm{m}^2\,\mathrm{m}^{-2}$ for all the three vascular PFTs and $1.04\,\mathrm{m}^2\,\mathrm{m}^{-2}$ for the nonvascular (moss) PFT were comparable with $1.76\,\mathrm{m}^2\,\mathrm{m}^{-2}$ for the trees, shrubs, and herbs and $0.85\,\mathrm{m}^2\,\mathrm{m}^{-2}$ for the mosses measured optically by *Syed et al.* [2006] at the WPL.
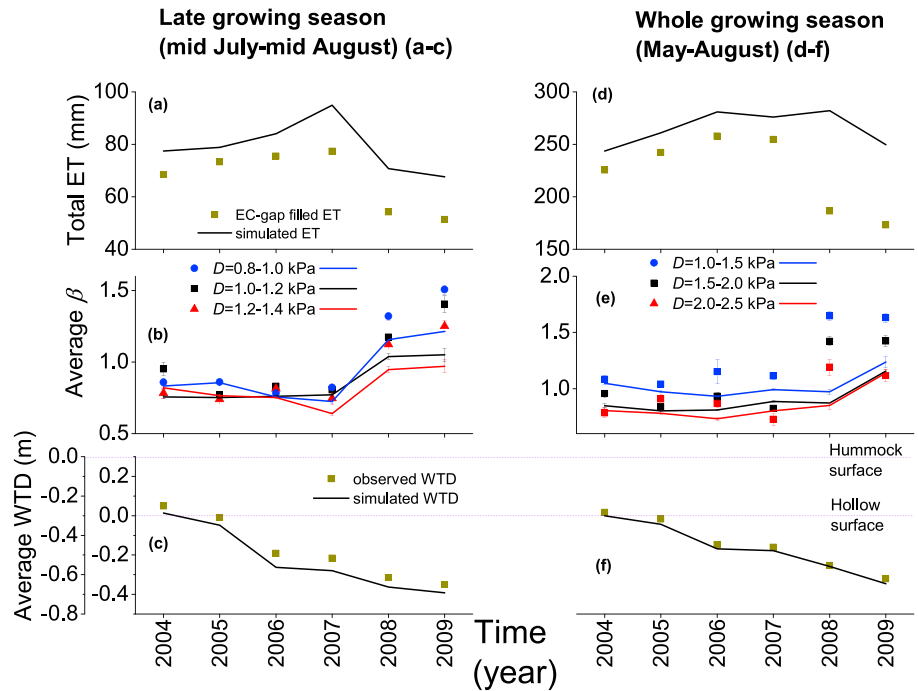
Figure 10. (a) Half hourly eddy covariance (EC) gap-filled [*Syed et al.*, 2006; *Flanagan and Syed*, 2011] and hourly modeled midday (2 h before and after solar noon) Bowen ratio (β); (b) hourly modeled vascular canopy water potential (ψ_c; on the left y axes) and canopy stomatal conductance (g_c; on the right y axes); and (c) hourly modeled moss (nonvascular) ψ_c during August 2005, 2008, and 2009 at a Western Canadian fen peatland.

3.7. Modeled Versus Measured Effects of Interannual Variations in WTD on Surface Energy Exchange

Beside the seasonal variation in surface energy exchange as affected by seasonality in R_n and D, the interannual variation in surface energy balance at the WPL was also affected by that in the WTD. Shallow WTD (shallower than 0.1 m below the hollow surface) during the 3 day period in mid-August (section 2.2.5) of 2005 caused greater LE than H fluxes as also apparent from diurnal EC flux measurements (Figure 9). WTD drawdown to about 0.32 m below the hollow surface during the similar period with comparable R_n and D in 2008 caused a reduction in EC-measured LE fluxes with respect to H fluxes (Figure 9). Further recession of WTD to about 0.38 m in the same period of 2009 with comparable R_n and D further reduced EC-measured LE with respect to H fluxes, thus yielding a surface energy balance dominated by H fluxes (Figure 9). This shift of surface energy balance from LE dominated in 2005 to H dominated in 2009 under comparable R_n and D indicated soil surface drying with a deepening of WTD from about 0.1 to 0.4 m below the hollow surface (Figure 9). This was corroborated by increases in EC gap-filled midday (2 h before and after solar noon) β from about 0.5 in 2005 to above 1 in 2009, which was simulated well by *ecosys* (Figure 10a). This soil drying in *ecosys* was apparent in reductions of moss canopy water potentials (ψ_c; Figure 10c) that reduced evaporation (E) from mosses. *Ecosys* also simulated a smaller reduction in vascular ψ_c during deeper WTD periods of 2008 and 2009 but not enough to cause a decline in midday canopy g_c and hence T from the vascular canopies (Figure 10b).

These WTD effects on surface energy balance also contributed to a WTD threshold effect on interannual variations in late growing season (mid-July to mid-August) surface energy exchange. A sharp reduction in EC gap-filled ET and a concurrent rise in EC gap-filled midday β under clear sky (shortwave radiation $>$700 Wm^{-2}; section 2.2.5) from below to above unity (Figure 11b) from late growing season of 2007 to that of 2008 and 2009 (Figure 11a) was caused when the WTD fell more than ~0.35 m below the hollow surface (Figure 11c). However, rises in β in drier growing seasons could not only be affected by soil drying from WTD drawdown but also by increasing D. To account for the effect of D on β we examined average late and whole growing season midday β for three narrow D classes (section 2.2.5). Consistency of the rise in

Figure 11. (a and d) Modeled and eddy covariance (EC) gap-filled [*Syed et al.*, 2006; *Flanagan and Syed*, 2011] total late growing season (mid-July to mid-August) and whole growing season (May-August) evapotranspiration (ET), (b and e) modeled and EC gap-filled [*Syed et al.*, 2006; *Flanagan and Syed*, 2011] average late and whole growing season midday (2 h before and after solar noon) Bowen ratio (β) under clear-sky condition (incoming shortwave radiation >700 W m^{-2}) for three different vapor pressure deficit (*D*) classes for each period (i.e., $D = 0.8-1$, $1-1.2$, and $1.2-1.4$ kPa for late growing season and $D = 1-1.5$, $1.5-2$, and $2-2.5$ kPa for whole growing season), and (c and f) average modeled and measured late and whole growing season water table depth (WTD) during 2004–2009 at a Western Canadian fen peatland. A negative WTD represents a depth below hummock/hollow surface, and a positive WTD represents a depth above hummock/hollow surface.

midday β from below to above unity with WTD drawdown from the late growing seasons of 2007 to 2008 and 2009 in all of these three *D* classes suggested that this shift was controlled predominantly by soil drying as opposed to *D* (Figure 11b). Although *ecosys* simulated late growing season (mid-July to mid-August) reduction in ET and concurrent rise in midday β when WTD fell below a threshold value of ~0.35 m from the hollow surface (~0.65 m from the hummock surface), it did not simulate the large drop in whole growing season (May–August) ET and a concurrent rise in β from 2007 to 2008 and 2009 with a similar drop of growing season WTD below the threshold (Figures 8j versus 8m, and 8p, and 11d–11f). This modeled overestimation of ET in 2008 and 2009 was also apparent in larger slopes from modeled versus EC measured hourly *LE* fluxes compared to other years (Table 1). This overestimation of ET was mainly contributed by larger modeled versus measured ET during May–June in 2008 and 2009 compared to other years (Figures 8m and 8p). A slightly

Table 2. Average Eddy Covariance (EC) Gap-Filled and Modeled Water Use Efficiency (WUE), Vapor Pressure Deficit (*D*), Air Temperature (*T$_a$*), Relative Humidity (RH), and Energy Balance Closure Between June 2007 and June 2008 at a Western Canadian Peatland[a]

Time Period		June 2007	June 2008
WUE (g C kg^{-1} H$_2$O)	EC gap filled	3.82 ± 0.08	6.71 ± 0.13
	Modeled	4.17 ± 0.07	4.69 ± 0.09
D (kPa)	Observed	0.87 ± 0.02	0.99 ± 0.02
T$_a$ (°C)	Observed	16.37 ± 0.12	17.61 ± 0.12
RH (%)	Observed	59 ± 1	57 ± 1
Energy balance closure	EC gap filled	0.73	0.66
	Modeled	1.00	1.00

[a]WUE were calculated from the ratio of gross primary productivity (GPP) and evapotranspiration (ET). Details of both WUE and energy balance closure calculations are in section 2.2.5. The plus minus sign denotes the standard error of mean.

higher D and R_n (Figures 8k versus 8n, and 8l versus 8o; Table 2) during June 2008 than in June 2007 suggested that the potential ET would be greater in June 2008 than in June 2007. Consequently, the modeled actual ET was larger in June 2008 than in June 2007, but the EC gap-filled actual ET in June 2008 was about 45% less than that in June 2007 (Figures 8j versus 8m). Moreover, smaller EC gap-filled June ET in 2008 than in 2007 was not associated with a decreased EC-derived GPP. This caused a great difference in EC-derived WUE (=GPP/ET) between these two periods, whereas the modeled WUE was almost the same (Table 2). Consequently, on a growing season (May–August) basis, an increase in modeled GPP by $32\,\mathrm{g\,C\,m^{-2}}$ from 2007 to 2008 was also associated with an increase in modeled growing season ET by 6 mm (Figure 11d). On the contrary, an increase in EC-derived growing season GPP by $54\,\mathrm{g\,C\,m^{-2}}$ from 2007 to 2008 was associated with a substantial decrease in EC gap-filled growing season ET by 68 mm (Figure 11d).

4. Discussion

4.1. Hypothesis 1: Modeling Peat Moisture Retention by van Genuchten Model (VGM) Versus Modified Campbell Model (MCM)

The VGM moisture desorption function (equations (5) and (6)) better simulated water retention at ψ_m near saturation than did the MCM (equations (3a,b) and (4a,b)) due to its use of sigmoidal moisture retention curves that retain higher θ close to saturation (Figure 1). This ability in VGM was imparted by the shape parameter α (equation (6)) that was absent in the MCM (equations 3(a,b) and 4(a,b)) (Figure 1). Moreover, different combinations of the slope parameter n and the shape parameter α that arise from the differences in ρ_b and hence θ_s, $\theta_{v,fc}$, and $\theta_{v,wp}$ enabled VGM to simulate differential soil moisture desorption at different peat depths that was not simulated well by MCM (Figures 1, 2, and 3b). For instance, a smaller n and a larger α for the layer at 0.085–0.115 m depth compared to those for the layers at 0.065–0.085 and 0.115–0.135 m depths in VGM represented higher moisture retention in the former layer and consequently simulated more gradual moisture desorption in that layer with increasing WTD than in the latter layers (Figures 2 and 3). This enabled the VGM simulation of *ecosys* to simulate more gradual pore drainage and consequent higher θ at 0.1 m than at 0.075 and 0.125 m. This trend was also corroborated by the higher θ measured at 0.1 m depth than at 0.075 and 0.125 m depths of a hummock at the WPL (Figure 3a). This suggests that the VGM is a better model of water retention in peats than is MCM but at the cost of two additional parameters that require fitting to observations of water desorption. Similar to our study, *Weiss et al.* [1998] found VGM to be the most suitable peat moisture retention model while testing several well-known water retention models commonly applied to mineral soils to fit measured water retention data for different suction pressures for 38 undrained peat samples collected at four different depths. While comparing VGM versus Campbell models in parameterizing the peat moisture retention function in CLASS, *Letts et al.* [2000] showed that Campbell model could be used in simulating peat moisture retention at the expense of significant underestimation of peat moisture content close to saturation when compared to VGM.

Peats at 0.075, 0.1, and 0.125 m were not saturated even when observed θ in those layers remained consistently high ($>0.65\,\mathrm{m^3\,m^{-3}}$) during most of 2005 and April–June of 2007 (Figures 3a, 5e, and 5k). This lack of saturation was modeled by simulating rapid infiltration through macropores (B18–B22), thus indicating the importance of preferential flow in modeling northern peatland moisture retention. *Dimitrov et al.* [2010] and *Dettmann et al.* [2014] also showed how inclusion of preferential flow improved overall peat moisture retention simulation for northern peatland ecosystems. *Hogan et al.* [2006] measured very high vertical hydraulic conductivities for top 0.3 m peat compared to peat underneath in a central Saskatchewan fen peatland that was similar to the peatland under this study, further signifying importance of preferential flow in fen peatland hydrology.

4.2. Hypothesis 2: Modeling WTD Variations in a Boreal Fen

Decreasing vertical water influx (P) versus efflux (ET) along with decreasing lateral water influx (recharge) and increasing lateral water efflux (discharge) enabled *ecosys* to simulate the gradual WTD drawdown from 2004 to 2009 that was measured at the WPL (Figures 6 and 7). Lateral water gain from upland ecosystems during the wetter years is typical for fen hydrology and was also observed by *Flanagan and Syed* [2011] at the WPL site. We did not have any direct hourly or daily site measurements of lateral inflow or outflow of water to corroborate the simulated recharge or discharge. However, reasonably accurate simulation of changes in soil water storage (ΔWTD and $\Delta\theta$) and vertical water transfer (ET) indicated adequate simulation of lateral

inflow/outflow of water at the WPL. Although the method developed here for our point scale study to model ΔWTD in a northern fen peatland is subjected to assumption about boundary conditions (e.g., WTD_x) to accommodate for lateral water gains/losses as affected by regional drying, it could be avoided by scaling up such modeling to an entire watershed that solves for regional water and energy balance.

Despite significant improvement in peat moisture retention simulation above WT, VGM did not differ much with MCM in simulating WTD (Figure 3). This indicated that both VGM and MCM simulations of *ecosys* simulated similar matric water potentials at different depths while simulating very different peat moisture contents corresponding to those water potentials (equations (3a,b), (5), and (6)). During the wetter years, e.g., 2004 and 2005 with shallower WT, VGM simulated higher near-surface peat moisture contents and hence greater unsaturated hydraulic conductivities compared to MCM (B3–B7 and B16–B17) and so enabled more rapid moss evaporation (*E*) (E2, F1–F3, and F6). This enabled VGM to simulate larger *LE*, lower β (=*H/LE*), and higher ET in *ecosys* than did MCM, which was more consistent with the measured values (results not shown). So the improvement in peat moisture simulation by VGM compared to MCM enabled better simulation of changes in surface energy balance as WTD drawdown progressed from the wetter growing season of 2004 to the drier growing season of 2009 (e.g., Figure 9). Besides, accurately modeling peat moisture contents in the unsaturated zone enhanced better modeling of gas exchange and its effects on aerobic versus anaerobic carbon and nitrogen transformations and hence carbon accumulation (results not shown).

4.3. Hypothesis 3: Modeling WTD Threshold Effects on Surface Energy Exchange

A WTD threshold effect on late growing season (mid-July to mid-August) surface energy exchange was apparent in EC measurements at the WPL. When WTD fell below ~0.35 m from the hollow surface (below 0.65 m from the hummock surface), EC gap-filled surface energy balance shifted from *LE* to *H* flux dominated and concurrently midday EC gap-filled β rose from below to above unity (Figures 9, 10a, and 11a–11c). *Ecosys* successfully simulated this WTD threshold effect on interannual variations in late growing season surface energy exchange by simulating different patterns of vertical rooting and water uptake between vascular (trees and shrubs) and nonvascular (moss) vegetation. Root growth in *ecosys* was driven by shoot-root C transfer in individual plants, which was then scaled to the population. Moss population were larger (section 2.2.3), and hence, intraspecific competition was greater so that individual moss plants and hence the downward growth of mosses below the ground were smaller than those of vascular roots (G9). This resulted in a modeled moss depth of 0.115 m below the hummock surface and 0.05 m below the hollow surface as opposed to modeled maximum vascular root depth of 0.65 m below the hummock surface and 0.35 m below the hollow surface. Reduced availability of [O_{2s}] in deeper wet peat layers and lack of O_2 transport through aerenchyma further limited modeled moss belowground growth to near-surface peat layers (G9). When WTD fell below ~0.35 m from the hollow surface (~0.65 m from the hummock surface), the near-surface peats drained from the VGM desorption curve in Figure 1, thereby decreasing θ, ψ_m (equation (6)), and hence ψ_s, soil matrix hydraulic conductivity (K_{mat}; B16), and increasing soil hydraulic resistance (Ω_s; F3) in those layers. Reduced K_{mat} hindered recharge of those layers through capillary rise (B2–B5) from the WT below, thereby further reducing ψ_s and increasing Ω_s in those layers. Reductions in ψ_s combined with increase in Ω_s thus reduced moss U_w (F2) that forced a reduction in moss canopy water potential (ψ_c; Figure 10c) and hence E from moss surface while equilibrating moss U_w with moss E (F6). Various field- and modeling-based studies [e.g., *Lafleur et al.*, 2005; *Sonnentag et al.*, 2010; *Dimitrov et al.*, 2011; *Peichl et al.*, 2014] have demonstrated reductions in moss E when capillary rise from WT deeper than a threshold depth was inadequate to support moss hydration in northern peatlands. The threshold WTD for reductions in ET across these peatlands varied from ~0.3 m [*Sonnentag et al.*, 2010] to ~0.65 m [*Lafleur et al.*, 2005] below the hummock surface depending upon the maximum depth at which capillary rise could support moss hydration. The maximum height of capillary rise is again controlled by the peat soil moisture retention properties, thereby yielding greater capillary rise from deeper WT in peats with high rather than low moisture-holding capacity. For instance, *Parmentier et al.* [2009] found no reduction in a Dutch peatland ET with WTD drawdown from peat surface level (0 m) to 0.51 m below the surface, which they attributed to high water-holding capacity of peats above WT. Peat water content at 0–0.15 m in their study only reduced from 0.89 to 0.72 $m^3\,m^{-3}$ with a reduction of soil water matric potential from saturation (0 MPa) to -0.01 MPa.

Unlike the moss PFT, the three vascular PFTs in *ecosys* could grow their roots into the wet deeper peat layers immediately above the WT. Deeper rooting in those vascular PFTs was simulated from enhanced root mass

growth and elongation (G8–G9) facilitated by greater root growth respiration (G4–G5 and G7) that was modeled from a combination of less intraspecific competition within lower populations (G9) and hence larger individual plant size and by improved root O_2 status ($[O_{2r}]$) in the deeper wet layers from O_2 transport through aerenchyma facilitated by root porosity (θ_{pr}) inputs of 0.1 and 0.3 (G3–G5, G7, and G9; section 2.2.3). The near-surface peat drying under WTD below ~0.35 from the hollow surface (~0.65 m from the hummock surface) also increased vascular root Ω_r and Ω_a and hence reduced vascular U_w from those layers (F2 and F4–F5) as for mosses. However, deeper rooting enabled *ecosys* to simulate root U_w from those deeper layers with high θ and ψ_s and low Ω_s, Ω_r, and Ω_a (F2–F5) that offset the reduction in near-surface root U_w. This offset enabled negligible reductions in vascular ψ_c and canopy g_c (Figure 10b) and hence sustained vascular T to be modeled when WTD was deeper than ~0.35 from the hollow surface (~0.65 from the hummock surface). As in our study, *Dimitrov et al*. [2011] modeled lack of vascular plant water stress in Mer Bleue bog, Canada, during deeper WT condition due to deeper rooting and sustained root water uptake, ψ_c and g_c. *Schwärzel et al*. [2006] also reported that in a drained fen peatland, deeper rooting combined with adequate capillary rise from the WT helped vascular plants to sustain water uptake and hence ET when WT dropped down to 0.7 m below the peat surface. However, sustained vascular T in our modeling could not offset the suppression of moss E when WTD fell below this threshold level of ~0.35 from the hollow surface (~0.65 m from the hummock surface).

4.4. Divergence Between Modeled and Measured Growing Season Energy Exchange

Divergence between modeled and measured growing season (May–August) ET in 2008 and 2009 (Figure 11 d) was mainly caused by larger modeled than measured ET during early growing season (May–June). Larger modeled versus EC gap-filled ET could partially be caused by lower-energy balance closure in EC gap-filled energy fluxes in those years (e.g., 2008–2009) as opposed to complete energy balance closure for all years in the model (Tables 1 and 2) forced by solutions to coupled energy balances and water transfer schemes (D1, E1, E3, E5, and E6) [*Grant and Flanagan*, 2007]. While examining eddy covariance energy balance closure in a similar boreal fen, *Barr et al*. [2012] showed that latent heat fluxes were twice as prone as sensible heat fluxes to undermeasurement. They also showed that applying an energy balance closure adjustment could increase measured evapotranspiration by 22% in that fen peatland. We further examined modeled versus measured soil-plant-atmosphere moisture relations to look for possible explanation for the lack of decline in modeled ET unlike EC gap-filled ET during early growing seasons of 2008 and 2009. Like site measurements, simulated near-surface θ during early growing season of 2008 (e.g., at 0.075, 0.1, and 0.125 m depth from the hummock surface; Figure 5n) remained well above the field capacity (Figure 2) sustained by WTD (within 0.2 m below the hollow surface) (Figure 5o) shallower than the threshold WTD below which surface energy exchange was affected in the model. These hydrological conditions provided adequate moisture to sustain higher modeled soil, moss, root, and canopy water potentials and conductances and hence larger modeled ET (B17, E2–E7, and F1–F6; equations (5) and (6)). Moreover, *ecosys* simulates stomatal effects on vascular transpiration and CO_2 fixation [*Grant and Flanagan*, 2007]. So a drought-induced reduction in transpiration through stomatal closure in the model would be accompanied by a commensurate reduction in vascular GPP. This allows a modeled vascular PFT in *ecosys* to conserve a fairly consistent WUE (GPP/ET) for a given D. Similar WUEs for vascular plant species growing under similar climates were also reported by *Larcher* [2003]. Beside vascular PFT, *ecosys* simulates reduction in moss photosynthetic rates with intense moss drying to represent cessation of rates of moss photosynthetic activity as a function of moss water potential. This can be corroborated by *Williams and Flanagan* [1996], who reported reductions in rates of net photosynthetic assimilation in dominant mosses growing at WPL site with reduction in moss water content. So a reduction in moss evaporation in the model would also be accompanied with a reduction in moss CO_2 fixation and GPP. Consequently, *ecosys* would not simulate a reduction in ET without commensurate reduction in GPP. This yielded a fairly consistent modeled WUE. On the contrary, abruptly high EC gap-filled WUE in 2008 versus 2007 was contributed by large decline in EC gap-filled ET, which was not associated with a commensurate decline in EC-partitioned GPP (Table 2 and section 3.7). *Brümmer et al*. [2012] also showed that a reduction or an increase in EC-derived GPP was associated with a commensurate increase or decrease in EC gap-filled ET over WPL during 2003–2006, thereby yielding a consistent WUE (GPP/ET = ~3 g C kg^{-1} H$_2$O) as modeled here (Table 2). So from our modeling we could not infer that the sharp decline in EC gap-filled ET during early growing seasons (May–June) of 2008 and 2009 was contributed by moss drying and/or vascular plant water stress due to deeper WT.

5. Conclusions

Our first objective was to examine whether *ecosys* could better simulate peat moisture retention in a northern boreal fen peatland when MCM was replaced by VGM. Our results showed that the higher near-saturation peat moisture retention can be better modeled by using the VGM desorption function that simulates sigmoidal (*S*-shape) moisture retention curves (Figures 1 and 3). We also examined whether the lateral boundary condition in a site-scale simulation in *ecosys* as defined by a specified external WTD (WTD_x) to some distance (L_t) can simulate lateral inflow and/or outflow of water and hence seasonal and interannual variations in a northern boreal fen WTD. Our results showed that hydraulically driven lateral water transfer using Darcian flow with the specified WTD_x and L_t could reasonably well simulate the seasonal and interannual variations in WTD at the WPL as long as WTD_x was adjusted to represent larger watershed-scale effects of fen hydrology (Figures 5 and 7). Lastly, we examined whether *ecosys* could simulate and hence explain the ecosystem drying as manifested by changes in surface energy exchange with WTD drawdown in a boreal fen. Differential vascular versus nonvascular rooting profiles enabled *ecosys* to simulate a reduction in late growing season (mid-July to mid-August) ET and a concurrent rise in β that was measured at the WPL, indicating ecosystem drying when WTD fell below a threshold (~0.35 m below the hollow or ~0.65 m below the hummock surface; Figures 11a–11c). However, our modeling could not explain a large decline in growing season (May–August) ET and a concurrent rise in β from 2007 to 2008 over a shallower WTD (Figures 11d–11f and Table 2).

The algorithms used to simulate ecohydrological interactions in this boreal fen represented fundamental soil physical and biological processes that were derived from basic independent research. Hence, peatland ecohydrological modeling such as this would be replicable across other fen peatlands if informed by site-specific ecohydrological inputs (Figure 2 and section 2.2.3). Such modeling can also be scaled up with regional-, continental-, or global-level inputs of those parameters. Since hydrology largely governs the balance between peat production and decomposition and hence between peat aggradation and degradation, ecohydrological process-level modeling would thus be important to predict hydrological effects on boreal fen peatlands' carbon balance. The insights and the improved predictive capacity of simulating ecohydrological interactions in fen peatlands could therefore be used to predict how those peatlands would behave under future warmer and drier climates.

References

Baker, I., L. Prihodko, A. Denning, M. Goulden, S. Miller, and H. Da Rocha (2008), Seasonal drought stress in the Amazon: Reconciling models and observations, *J. Geophys. Res.*, 113, G00B01, doi:10.1029/2007JG000644.

Barr, A. G., G. Van der Kamp, T. A. Black, J. H. McCaughey, and Z. Nesic (2012), Energy balance closure at the BERMS flux towers in relation to the water balance of the White Gull Creek watershed 1999–2009, *Agric. For. Meteorol.*, 153, 3–13.

Boelter, D. (1969), Physical properties of peats as related to degree of decomposition, *Soil Sci. Soc. Am. Pro.*, 33, 606–609.

Boelter, D. (1970), Important physical properties of peat materials, in *3rd International Peat Congress Proceedings*, pp. 150–154, Helsinki, Finland.

Bond-Lamberty, B., S. T. Gower, and D. E. Ahl (2007), Improved simulation of poorly drained forests using Biome-BGC, *Tree Physiol.*, 27, 703–715.

Brümmer, C., T. A. Black, R. S. Jassal, N. J. Grant, D. L. Spittlehouse, B. Chen, Z. Nesic, B. D. Amiro, M. A. Arain, and A. G. Barr (2012), How climate and vegetation type influence evapotranspiration and water use efficiency in Canadian forest, peatland and grassland ecosystems, *Agric. For. Meteorol.*, 153, 14–30.

Cai, T., L. B. Flanagan, and K. H. Syed (2010), Warmer and drier conditions stimulate respiration more than photosynthesis in a boreal peatland ecosystem: analysis of automatic chambers and eddy covariance measurements, *Plant Cell Environ.*, 33, 394–407.

Campbell, G. S. (1974), A simple method for determining unsaturated conductivity from moisture retention data, *Soil Sci.*, 117, 311–314.

Clymo, R. S., J. Turunen, and T. Tolonen (1998), Carbon accumulation in peat, *Oikos*, 81, 368–388.

Cronk, J. K., and M. S. Fennessy (2001), *Wetland Plants: Biology and Ecology*, CRC Press, Florida.

Dettmann, U., M. Bechtold, E. Frahm, and B. Tiemeyer (2014), On the applicability of unimodal and bimodal van Genuchten–Mualem based models to peat and other organic soils under evaporation conditions, *J. Hydrol.*, 515, 103–115.

Dimitrov, D. D., R. F. Grant, P. M. Lafleur, and E. R. Humphreys (2010), Modeling the subsurface hydrology of Mer Bleue bog, *Soil Sci. Soc. Am. J.*, 74, 680–694.

Dimitrov, D. D., R. F. Grant, P. M. Lafleur, and E. R. Humphreys (2011), Modeling the effects of hydrology on gross primary productivity and net ecosystem productivity at Mer Bleue bog, *J. Geophys. Res.* 116, G04010, doi:10.1029/2010JG001586.

Dimitrov, D. D., J. S. Bhatti, and R. F. Grant (2014), The transition zones (ecotone) between boreal forests and peatlands: Modelling water table along a transition zone between upland black spruce forest and poor forested fen in central Saskatchewan, *Ecol. Model.*, 274, 57–70.

Dise, N. B. (2009), Peatland response to global change, *Science*, 326, 810.

Flanagan, L. B., and K. H. Syed (2011), Stimulation of both photosynthesis and respiration in response to warmer and drier conditions in a boreal peatland ecosystem, *Global Change Biol.*, 17, 2271–2287.

Frolking, S., N. T. Roulet, T. R. Moore, P. M. Lafleur, J. L. Bubier, and P. M. Crill (2002), Modeling seasonal to annual carbon balance of Mer Bleue Bog, Ontario, Canada, *Global Biogeochem. Cycles*, 16(3), 1030, doi:10.1029/2001GB001457.

Frolking, S., J. Talbot, M. C. Jones, C. C. Treat, J. B. Kauffman, E.-S. Tuittila, and N. Roulet (2011), Peatlands in the Earth's 21st century climate system, *Environ. Rev.*, 19, 371–396.

Gerten, D., S. Schaphoff, U. Haberlandt, W. Lucht, and S. Sitch (2004), Terrestrial vegetation and water balance—Hydrological evaluation of a dynamic global vegetation model, *J. Hydrol.*, *286*, 249–270.

Gnatowski, T., J. Szatyłowicz, T. Brandyk, and C. Kechavarzi (2010), Hydraulic properties of fen peat soils in Poland, *Geoderma*, *154*, 188–195.

Gorham, E., J. Janssens, and P. Glaser (2003), Rates of peat accumulation during the postglacial period in 32 sites from Alaska to Newfoundland, with special emphasis on northern Minnesota, *Can. J. Botany*, *81*, 429–438.

Grant, R., and L. Flanagan (2007), Modeling stomatal and nonstomatal effects of water deficits on CO_2 fixation in a semiarid grassland, *J. Geophys. Res. 112*, G03011, doi:10.1029/2006JG000302.

Grant, R., M. Amrani, D. Heaney, R. Wright, and M. Zhang (2004), Mathematical modeling of phosphorus losses from land application of hog and cattle manure, *J. Environ. Qual.*, *33*, 210–231.

Grant, R., A. Barr, T. Black, H. Margolis, A. Dunn, J. Metsaranta, S. Wang, J. McCaughey, and C. Bourque (2009), Interannual variation in net ecosystem productivity of Canadian forests as affected by regional weather patterns—A Fluxnet-Canada synthesis, *Agric. For. Meteorol.*, *149*, 2022–2039.

Grant, R., A. Desai, and B. Sulman (2012), Modelling contrasting responses of wetland productivity to changes in water table depth, *Biogeosciences*, *9*, 4215–4231.

Hogan, J. M., G. Van der Kamp, S. L. Barbour, and R. Schmidt (2006), Field methods for measuring hydraulic properties of peat deposits, *Hydrol. Process.*, *20*, 3635–3649.

Kellner, E. (2001), Surface energy fluxes and control of evapotranspiration from a Swedish *Sphagnum* mire, *Agric. For. Meteorol.*, *110*, 101–123.

Krinner, G., N. Viovy, N. de Noblet-Ducoudré, J. Ogée, J. Polcher, P. Friedlingstein, P. Ciais, S. Sitch, and I. C. Prentice (2005), A dynamic global vegetation model for studies of the coupled atmosphere-biosphere system, *Global Biogeochem. Cyles*, *19*, GB1015, doi:10.1029/2003GB002199.

Kurbatova, J., C. Li, F. Tatarinov, A. Varlagin, N. Shalukhina, and A. Olchev (2009), Modeling of the carbon dioxide fluxes in European Russia peat bogs, *Environ. Res. Lett.*, *4*, 045022.

Lafleur, P. M., R. A. Hember, S. W. Admiral, and N. T. Roulet (2005), Annual and seasonal variability in evapotranspiration and water table at a shrub-covered bog in southern Ontario, Canada, *Hydrol. Process.*, *19*, 3533–3550.

Larcher, W. (2003), *Physiological Plant Ecology*, 4th ed., Springer, Berlin.

Letts, M. G., N. T. Roulet, N. T. Comer, M. R. Skarupa, and D. L. Verseghy (2000), Parametrization of peatland hydraulic properties for the Canadian Land Surface Scheme, *Atmos. Ocean*, *38*, 141–160.

Long, K. D. (2008), Methane fluxes from a northern peatland: mechanisms controlling diurnal and seasonal variation and the magnitude of aerobic methanogenesis, M.Sc. thesis, Department of Biological Sciences, Univ. of Lethbridge, Lethbridge, Alberta, Canada.

Long, K. D., L. B. Flanagan, and T. Cai (2010), Diurnal and seasonal variation in methane emissions in a northern Canadian peatland measured by eddy covariance, *Global Change Biol.*, *16*, 2420–2435.

Mezbahuddin, M., R. F. Grant, and T. Hirano (2014), Modelling effects of seasonal variation in water table depth on net ecosystem CO_2 exchange of a tropical peatland, *Biogeosciences*, *11*, 577–599.

Mezbahuddin, M., R. F. Grant, and T. Hirano (2015), How hydrology determines seasonal and interannual variations in water table depth, surface energy exchange, and water stress in a tropical peatland: Modeling versus measurements, *J. Geophys. Res. Biogeosci.*, *120*, 2132–2157, doi:10.1002/2015JG003005.

Päivänen, J. (1973), Hydraulic conductivity and water retention in peat soils, *Acta For. Fen.*, *129*, 1–70.

Parmentier, F., M. van der Molen, R. de Jeu, D. Hendriks, and A. Dolman (2009), CO_2 fluxes and evaporation on a peatland in the Netherlands appear not affected by water table fluctuations, *Agric. For. Meteorol.*, *149*, 1201–1208.

Peichl, M., M. Öquist, M. O. Löfvenius, U. Ilstedt, J. Sagerfors, A. Grelle, A. Lindroth, and M. B. Nilsson (2014), A 12-year record reveals pre-growing season temperature and water table level threshold effects on the net carbon dioxide exchange in a boreal fen, *Environ. Res. Lett.*, *9*, 055006.

Richardson, A. D., D. Y. Hollinger, G. G. Burba, K. J. Davis, L. B. Flanagan, G. G. Katul, J. W. Munger, D. M. Ricciuto, P. C. Stoy, and A. E. Suyker (2006), A multi-site analysis of random error in tower-based measurements of carbon and energy fluxes, *Agric. For. Meteorol.*, *136*, 1–18.

Roulet, N. T., P. M. Lafleur, P. J. H. Richard, T. R. Moore, E. R. Humphreys, and J. Bubier (2007), Contemporary carbon balance and late Holocene carbon accumulation in a northern peatland, *Global Change Biol.*, *13*, 397–411.

Schaefer, K., G. J. Collatz, P. Tans, A. S. Denning, I. Baker, J. Berry, L. Prihodko, N. Suits, and A. Philpott (2008), Combined simple biosphere/Carnegie-Ames-Stanford approach terrestrial carbon cycle model, *J. Geophys. Res.*, *113*, G03034, doi:10.1029/2007JG000603.

Schwärzel, K., J. Šimůnek, M. T. van Genuchten, and G. Wessolek (2006), Measurement modeling of soil-water dynamics evapotranspiration of drained peatland soils, *J. Plant Nutr. Soil Sc.*, *169*, 762–774.

Silins, U., and R. L. Rothwell (1998), Forest peatland drainage and subsidence affect soil water retention and transport properties in an Alberta peatland, *Soil Sci. Soc. Am. J.*, *62*, 1048–1056.

Sitch, S., B. Smith, I. C. Prentice, A. Arneth, A. Bondeau, W. Cramer, J. Kaplan, S. Levis, W. Lucht, and M. T. Sykes (2003), Evaluation of ecosystem dynamics, plant geography and terrestrial carbon cycling in the LPJ dynamic global vegetation model, *Global Change Biol.*, *9*, 161–185.

Sonnentag, O., J. Chen, N. Roulet, W. Ju, and A. Govind (2008), Spatially explicit simulation of peatland hydrology and carbon dioxide exchange: Influence of mesoscale topography, *J. Geophys. Res.*, *113*, G02005, doi:10.1029/2007JG000605.

Sonnentag, O., G. van der Kamp, A. Barr, and J. Chen (2010), On the relationship between water table depth and water vapor and carbon dioxide fluxes in a minerotrophic fen, *Global Change Biol.*, *16*, 1762–1776.

St-Hilaire, F., J. Wu, N. T. Roulet, S. Frolking, P. M. Lafleur, E. R. Humphreys, and V. Arora (2010), McGill wetland model: evaluation of a peatland carbon simulator developed for global assessments, *Biogeosciences*, *7*, 3517–3530.

Sulman, B. N., A. R. Desai, N. Z. Saliendra, P. M. Lafleur, L. B. Flanagan, O. Sonnentag, D. S. Mackay, A. G. Barr, and G. van der Kamp (2010), CO_2 fluxes at northern fens and bogs have opposite responses to inter-annual fluctuations in water table, *Geophys. Res. Lett.*, *37*, L19702, doi:10.1029/2010GL044018.

Sulman, B. N., A. R. Desai, N. M. Schroeder, D. Ricciuto, A. Barr, A. D. Richardson, L. B. Flanagan, P. M. Lafleur, H. Tian, and G. Chen (2012), Impact of hydrological variations on modeling of peatland CO_2 fluxes: Results from the North American Carbon Program site synthesis, *J. Geophys. Res.*, *117*, G01031, doi:10.1029/2011JG001862.

Sulman, B., A. Desai, B. Cook, N. Saliendra, and D. Mackay (2009), Contrasting carbon dioxide fluxes between a drying shrub wetland in Northern Wisconsin, USA, and nearby forests, *Biogeosciences*, *6*, 1115–1126.

Syed, K. H., L. B. Flanagan, P. J. Carlson, A. J. Glenn, and K. E. van Gaalen (2006), Environmental control of net ecosystem CO_2 exchange in a treed, moderately rich fen in northern Alberta, *Agric. For. Meteorol.*, *140*, 97–114.

Szymanowski, M. (1993), Basic physico-hydrological and retention properties and their relationship with bulk density of various weakly-sludged (low-ash) peat formations, *Wiadomości IMUZ*, *17*, 153–174.

Tarnocai, C. (2006), The effect of climate change on carbon in Canadian peatlands, *Global Planet. Change*, *53*, 222–232.

Tian, H., G. Chen, M. Liu, C. Zhang, G. Sun, C. Lu, X. Xu, W. Ren, S. Pan, and A. Chappelka (2010), Model estimates of net primary productivity, evapotranspiration, and water use efficiency in the terrestrial ecosystems of the southern United States during 1895-2007, *Forest Ecol. Manag.*, *259*, 1311–1327.

Turunen, J., N. T. Roulet, T. R. Moore, and P. J. H. Richard (2004), Nitrogen deposition and increased carbon accumulation in ombrotrophic peatlands in eastern Canada, *Global Biogeochem. Cyles*, *18*, GB3002, doi:10.1029/2003GB002154.

van Genuchten, M. T. (1980), A closed-form equation for predicting the hydraulic conductivity of unsaturated soils, *Soil Sci. Soc. Am. J.*, *44*, 892–898.

van Genuchten, M. T., F. Leij, and S. Yates (1991), The RETC code for quantifying the hydraulic functions of unsaturated soils, Robert S. Kerr Environmental Research Laboratory.

van Huissteden, J., R. van den Bos, and I. M. Alvarez (2006), Modelling the effect of water-table management on CO_2 and CH_4 fluxes from peat soils, *Neth. J. Geosci.*, *85*, 3–18.

Vitt, D. H., L. A. Halsey, I. E. Bauer, and C. Campbell (2000), Spatial and temporal trends in carbon storage of peatlands of continental western Canada through the Holocene, *Can. J. Earth Sci.*, *37*, 683–693.

Weiss, R., J. Alm, R. Laiho, and J. Laine (1998), Modeling moisture retention in peat soils, *Soil Sci. Soc. Am. J.*, *62*, 305–313.

Weng, E., and Y. Luo (2008), Soil hydrological properties regulate grassland ecosystem responses to multifactor global change: A modeling analysis, *J. Geophys. Res. 113*, G03003, doi:10.1029/2007JG000539.

Wesely, M. L., and R. L. Hart (1985), Variability of short term eddy-correlation estimates of mass exchange, in *The Forest-Atmosphere Interaction*, edited by B. A. Hutchinson, B. B. Hicks, and D. Reidel, pp. 591–612, Springer, Dordrecht, Netherlands.

Wever, L. A., L. B. Flanagan, and P. J. Carlson (2002), Seasonal and interannual variation in evapotranspiration, energy balance and surface conductance in a northern temperate grassland, *Agric. For. Meteorol.*, *112*, 31–49.

Williams, T. G., and L. B. Flanagan (1996), Effect of changes in water content on photosynthesis, transpiration and discrimination against $^{13}CO_2$ and $C^{18}O^{16}O$ in *Pleurozium* and *Sphagnum*, *Oecologia*, *108*, 38–46.

Willmott, C. J. (1981), On the validation of models, *Phys. Gogr.*, *2*, 184–194.

Willmott, C. J. (1982), Some comments on the evaluation of model performance, *Bull. Am. Meteorol. Soc.*, *63*, 1309–1313.

Willmott, C. J., and D. E. Wicks (1980), An empirical method for the spatial interpolation of monthly precipitation within California, *Phys. Gogr.*, *1*, 59–73.

Wilson, K., A. Goldstein, E. Falge, M. Aubinet, D. Baldocchi, P. Berbigier, C. Bernhofer, R. Ceulemans, H. Dolman, and C. Field (2002), Energy balance closure at FLUXNET sites, *Agric. For. Meteorol.*, *113*, 223–243.

Wösten, J., E. Clymans, S. Page, J. Rieley, and S. Limin (2008), Peat–water interrelationships in a tropical peatland ecosystem in Southeast Asia, *Catena*, *73*, 212–224.

Wu, J., and N. T. Roulet (2014), Climate change reduces the capacity of northern peatlands to absorb the atmospheric carbon dioxide: The different responses of bogs and fens, *Global Biogeochem. Cycles*, *28*, 1005–1024, doi:10.1002/2014GB004845.

Wu, J., L. Kutzbach, D. Jager, C. Wille, and M. Wilmking (2010), Evapotranspiration dynamicsin a boreal peatland and its impact on the water and energy balance, *J. Geophys. Res.*, *115*, G04038, doi:10.1029/2009JG001075.

Wu, J., N. T. Roulet, M. Nilsson, P. Lafleur, and E. Humphreys (2012), Simulating the carbon cycling of northern peatlands using a land surface scheme coupled to a wetland carbon model (CLASS3W-MWM), *Atmos. Ocean*, *50*, 487–506.

Zhang, Y., C. Li, C. C. Trettin, H. Li, and G. Sun (2002), An integrated model of soil, hydrology, and vegetation for carbon dynamics in wetland ecosystems, *Global Biogeochem. Cycles.*, *16*(4), 1061, doi:10.1029/2001GB001838.

Zoltai, S. C., and D. H. Vitt (1990), Holocene climatic change and the distribution of peatlands in western interior Canada, *Quat. Res.*, *33*, 231–240.